Journal for ImmunoTherapy of Cancer

In situ endoscopic photodynamic therapy combined with immature DC vaccination induces a robust T cell response against peritoneal carcinomatosis

Charline Degavre,[1] Anouk Lepez,[1] Sebastien Ibanez,[1] Clémence François,[1] Katarzyna Głowacka,[1] Céline Guilbaud,[1] Florine Laloux-Morris,[1] Hrag Esfahani,[2] Davide Brusa,[3] Caroline Bouzin,[4] Olivier Feron [1,5]

To cite: Degavre C, Lepez A, Ibanez S, *et al*. In situ endoscopic photodynamic therapy combined with immature DC vaccination induces a robust T cell response against peritoneal carcinomatosis. *Journal for ImmunoTherapy of Cancer* 2024;**12**:e009752. doi:10.1136/jitc-2024-009752

► Additional supplemental material is published online only. To view, please visit the journal online (https://doi.org/10.1136/jitc-2024-009752).

Accepted 20 October 2024

For numbered affiliations see end of article.

Correspondence to
Professor Olivier Feron;
olivier.feron@uclouvain.be

ABSTRACT

Background Immunogenic cell death (ICD) and ferroptosis have recently emerged as key factors in the anticancer immune response. Among the treatments able to induce ICD and the associated release of danger signals is photodynamic therapy (PDT). Ferroptosis for its part results from lipid peroxidation and is induced by $CD8^+$ T cells to kill nearby cancer cells on IFN-γ production. We aimed to combine the two concepts, that is, to evaluate whether the strong pro-oxidant effects of PDT may promote ferroptosis and antigen release and to develop a procedure for in situ PDT to prepare the soil for highly endocytotic immature dendritic cell (iDC) adoptive transfer. This approach was implemented for managing peritoneal carcinomatosis, a lesion often associated with poor outcomes.

Methods We used three-dimensional (3D) heterotypic spheroids made of cancer cells, exposed them to a white light-activated OR141 photosensitizer (PS), and subsequently complexified them by adding iDC and naive lymphocytes. We next used a model of mouse peritoneal carcinomatosis and administered PDT using laparoscopy to locally induce photoactivation using the endoscope light. The immune response following adoptive transfer of iDC was tracked both in vivo and ex vivo using isolated immune cells from in situ vaccinated mice.

Results Cancer cells undergoing PDT-induced cell death significantly increased ICD markers and the infiltration of iDCs in spheroids, relying on ferroptosis. These actions induced the sequential activation of $CD8^+$ and $CD4^+$ T cells as revealed by a significant spheroid 3D structure deterioration and, remarkably, were not recapitulated by conventional ferroptosis inducer RSL3. Using LED light from an endoscope for in situ photoactivation of PS enabled us to apply the vaccination modality in mice with peritoneal tumors. Consecutive intraperitoneal injection of iDCs resulted in delayed tumor growth, increased survival rates, and prevented tumor relapse on rechallenge. $CD8^+$ T cell response was supported by depletion experiments, nodal detection of early activated T cells, and ex vivo T cell-induced cytotoxicity toward spheroids.

Conclusions The combination of in situ PDT locally delivered by an endoscope light and iDC administration induces a durable memory immune response against peritoneal carcinomatosis thereby opening new perspectives for the treatment of a life-threatening condition.

WHAT IS ALREADY KNOWN ON THIS TOPIC

⇒ There is a current renewed rise in anticancer vaccination approaches, especially now as certain limitations inherent to immune checkpoint blockers and CAR T cells are gradually being reached. One major trend is to engineer dendritic cell (DC) in vitro to promote their maturation while loading them with specific tumor antigens before reinjection to cancer patients.

WHAT THIS STUDY ADDS

⇒ This work pushes the concept of in situ vaccination by DCs beyond the options typically considered, as we report an innovative photodynamic therapy-based combination of in situ induction of an immunogenic tumor environment and concomitant release of a very broad repertoire of anonymous antigens, with the in situ transfer of immature DCs that do not need to be engineered or preloaded with tumor antigens.

HOW THIS STUDY MIGHT AFFECT RESEARCH, PRACTICE OR POLICY

⇒ The successful demonstration of endoscope light activating a photosensitizer in situ (via intraperitoneal laparoscopy) alongside the use of immature DCs—avoiding costly and complex production procedures—presents promising clinical opportunities. This advancement opens avenues to elicit a strong memory immune response against peritoneal carcinomatosis, a currently unmet need for many patients whose cancer progresses in the abdominal cavity.

INTRODUCTION

Anticancer dendritic cell (DC) vaccination is an immunotherapeutic approach that harnesses the power of the body's own immune system to fight tumors.[1–3] By

presenting tumor antigens (TAs) to T cells, DCs activate and educate immune cells to recognize and attack cancer cells.[4] The most common vaccination protocol is based on DC harvesting from the cancer patient and consecutive in vitro loading with TAs before reintroduction into the patient.[5] Response rates of DC vaccination, however, rarely surpass 15%,[6] and only one such product, Sipuleucel-T, has received FDA (Food and Drug Administration) approval to date.[7] While these modalities offer the possibility of tailoring DC vaccination to individual patients, there are constraints regarding the identity and amount of TAs presented by DCs that will ultimately support an efficient T cell response on transfer back to the patient. Another hurdle is the cost of both DC engineering in GMP facilities and molecular assays required for patient stratification (to identify those most likely to benefit from vaccination).[8]

A more straightforward strategy might, therefore, consist in the use of DCs that would be exposed in situ to tumors prechallenged to acutely release a maximum of antigens covering the large proteomic diversity of cancer cells, also called anonymous antigens.[9 10] Interestingly, while the endocytotic process is downregulated in mature DCs (to avoid the presentation of self-antigens encountered before activation), immature DCs (iDCs) have the potential to avidly capture antigens through a variety of mechanisms, including macropinocytosis and receptor-mediated paths.[11] We, therefore, reasoned that imposing a spatial constraint to iDCs during the exposure to TAs might curb tolerance development and be favorable to a consecutive anticancer T cell response. Induction of immunogenic cell death (ICD) could meet these criteria since it combines the local release of antigens by killed cancer cells and the creation of an environment prone to an immune response. The peritoneal cavity could represent such a spatial delineation to target local tumors with an ICD-inducing modality and to introduce highly endocytotic iDCs without any requirements to mature or engineer them. This site is actually of major therapeutic importance, as peritoneal carcinomatosis has a significant negative impact on the progression of various abdominal cancers and currently represents an unmet medical need.

Photodynamic therapy (PDT) is among the most potent inducers of ICD.[12–15] We have previously reported that potent vaccine may be generated by exposing in vitro iDCs to PDT-killed cancer cells.[16 17] PDT involves the use of a photosensitizer (PS) that is activated on light exposure. While most porphyrinic PSs are activated by specific wavelengths of light, others respond to the full spectrum of white light, including OR141, a non-porphyrinic PS that we previously identified.[18] Although this may appear as a significant hurdle in terms of penetration of light into tissues, we have shown that following systemic administration of OR141 in tumor-bearing mice,[18] substantial growth inhibitory effects are observed when subcutaneous tumors are exposed to an external LED lamp placed a few centimeters away from the skin of the animal.[13 19] This observation prompted us to explore, here, the possibility to use the white light of an endoscope inserted during laparoscopy to deliver PDT into the peritoneal cavity and thereby exert in situ cytotoxic effects toward a local tumor but also preparing the soil for subsequent iDC administration.

Interestingly, PDT was recently reported to promote ferroptosis in response to the high pro-oxidant stimulus resulting from the generation of singlet oxygen and more conventional ROS.[15 20–22] These data led us and other investigators to hypothesize that ferroptotic cell death triggered by PDT is immunogenic, thereby offering an explanation to anterior studies supporting the potential of combining PDT and DC vaccination.[23 24] This hypothesis was further supported by breakthrough studies demonstrating that ferroptosis directly participates in the cytotoxic effects of activated T cells.[25 26] By contrast, evaluation of the immunogenicity of ferroptosis itself led to contrasted results with a study documenting that ferroptotic cancer cells were poorly engulfed, dampening antigen cross-presentation,[27] while others investigators reported a strong immune response although possibly dependent on the biological context.[28–30] In addition to our objective of implementing a laparoscopic methodology of in situ PDT protocol in combination with iDC vaccination, we, therefore, added ferroptosis as a second point of attention in the mechanistic dissection of DC-based immune response. This led us to identify ferroptosis as a necessary but not sufficient component of PDT involved in the priming of peritoneal carcinomatosis before iDC transfer and to validate the use of the endoscope white light as an efficient modality to locally photoactivate PS OR141 and induce a consecutive DC-mediated anti-cancer T cell response.

RESULTS

PDT exerts cytotoxic effects on three-dimensional tumor spheroids and cancer cells through ferroptosis

To integrate the possible influence of the microenvironment on the type of cell death induced by non-porphyrinic PS OR141,[18] we first worked with three-dimensional (3D) spheroids to mimic biological gradients in tumors (such as nutrients, oxygen, and metabolic wastes) and address the issues of PS diffusion and light penetration. We first used 3D spheroids made of colorectal CT26 cancer cells, treated or not with one of the following drugs (used at the maximal non-toxic concentration when used alone): a pan-caspase inhibitor of apoptosis (zVAD-fmk), a kinase RIP1 inhibitor of necroptosis (necrostatin-1), or ferrostatin-1, a radical-trapping antioxidant inhibiting ferroptosis.[31] Ferroptosis was the major contributor to cell death induced by photoactivation of OR141, as ferrostatin-1 considerably decreased cytotoxicity over time at the different PS concentrations while necroptosis and apoptosis inhibitors failed to do so (figure 1A). A shift to the right of the dose-response curve was also observed in the presence of ferrostatin-1 confirming the role of lipid ROS in the PDT-induced cell death (figure 1B). Similar results

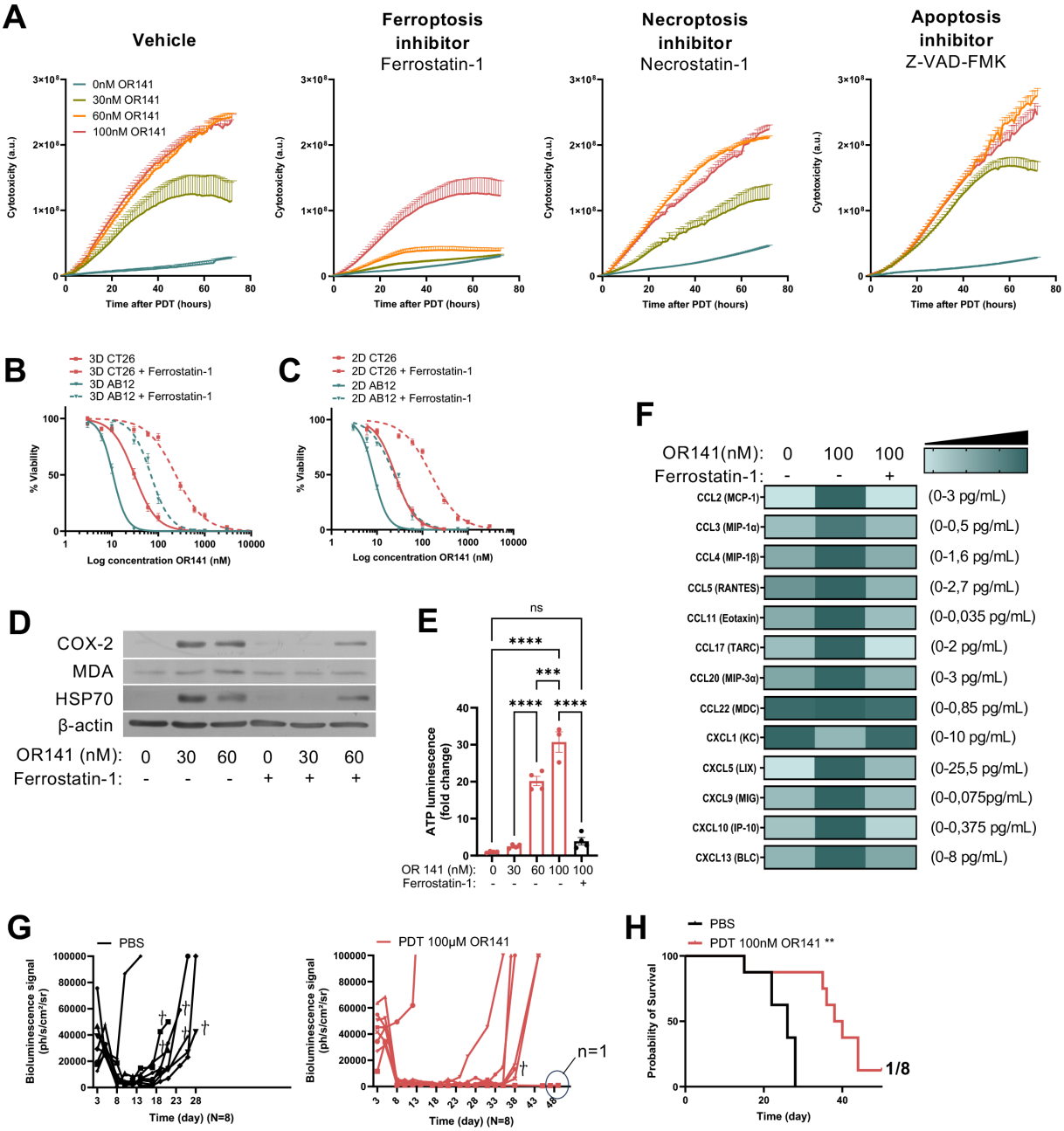

Figure 1 PDT induces ferroptosis and immunogenic cell death. (A–F) CT26 colorectal carcinoma and AB12 mesothelioma two-dimensional (2D) cell cultures and 3D spheroids were treated with the following drugs: ferrostatin-1 (10 µM), liproxstatin-1 (10 µM), necrostatin-1 (20 µM for 2D and 30 µM for 3D), Zvad-fmk (25 µM for 2D or 40 µM for 3D). After 48 hours pretreatment, cell cultures or spheroids were incubated with PS-OR141 in the dark for 1 hour (2D) or 4 hours (3D) at the indicated concentrations, followed by a washing step. Photoactivation was performed using an LED light source for 60 min (2D) or 90 min (3D) and incubation was continued after the renewal of cell death inhibitors. (A) PDT-induced cytotoxicity over time in CT26 spheroids (cytotox green dye, Incucyte) in the presence of different cell death inhibitors. (B, C) Dose-response curves depicting the viability of CT26 and AB12 (B) 3D spheroid (propidium iodide measurement by flow cytometry) and (C) 2D cell monolayers (PrestoBlue) 48 hours and 24 hours post-PDT, respectively, in the presence of 10 µM ferrostatin-1. (D) Representative COX2, HSP70, MDA and β-actin immunoblots from CT26 spheroids collected 20 hours post-PDT. (E) Extracellular ATP release from CT26 spheroids (expressed as fold change) was determined 30 min post-PDT. (F) Heat map of LEGENDplex proinflammatory chemokines (13-plex) released by CT26 spheroids 3 hours post-PDT. N=2. (G, H) Prophylactic vaccination model. Mice were injected s.c. with 1×10^6 luc$^+$ AB1 2D cells exposed in vitro to photoactivated 100 nM PS-OR141 (or PBS as control) and challenged 1 week later with i.p. injection of live 1×10^6 luc$^+$ AB1 cells. (G) Tumor burden monitored by bioluminescence (expressed as photons/s/cm^2/sr) and (H) corresponding survival curves. (**p≤0.01, N=8 mice per group). In vitro data (B, C, E) are plotted as the means±SEM from 3 independent experiments performed with ≥3 technical replicates (***p≤0.001; ****p≤0.0001; ns, p>0.05); when spheroids are involved, minimum of 6 spheroids were pooled together per condition. Significance was determined by one-way ANOVA with Tukey's multiple comparison test. Log-rank (Mantel-Cox) test was used for survival curves. ANOVA, analysis of variance; i.p., intraperitoneal; PDT, photodynamic therapy.

were obtained with spheroids made of AB12 mesothelioma cells (another cancer type prone to peritoneal carcinomatosis) that were slightly more sensitive to PDT effects than CT26 spheroids (figure 1B). We repeated these experiments in CT26 and AB12 cancer cells cultured as 2D monolayers and found the same profile of response and sensitivity to ferroptosis inhibitors ferrostatin-1 and liproxstatin-1 (figure 1C and online supplemental figure 1A). By contrast, as observed in 3D spheroids, necroptosis and apoptosis inhibitors failed to dampen PDT-induced cytotoxicity (online supplemental figure 1B). Annexin V/7-AAD flow cytometry cell death analysis further confirmed that activated PS dose-dependently induces cell death in a ferrostatin-dependent manner (see upper right quadrants in online supplemental figure 1C). Necrostatin-1 and Z-VAD-FMK did not reduce the extent of double positive dead cells (and even increased it a bit). A modest, dose-dependent increase in Annexin V-positive cells (lower right quadrant), slightly inhibited by Z-VAD-FMK, was observed, suggesting a marginal proapoptotic effect of PDT in addition to its prominent proferroptotic mode of cell death (online supplemental figure 1C). As further support of photoactivated PS-induced ferroptosis, we found that PDT triggered induction of COX2, considered as a biomarker of ferroptosis, and heat shock protein 70, an oxidative stress marker, along with an increase in malondialheyde (MDA) signal, a secondary product of lipid peroxidation (figure 1D); the PDT-induced upregulation of these markers was prevented in the presence of ferrostatin-1 (figure 1D). Besides Hsp70, we also looked for other markers of ICD, including the release of ATP, a well-known danger signal. We found that ATP release in the extracellular medium was dose-dependently increased in response to PDT (figure 1E). We were unable to detect calreticulin translocation (an “eat-me” signal) due to the extended time required for dissociation and staining of cells from 3D spheroids. However, it is worth noting that we had previously characterized its translocation in the same cancer cells cultured as monolayers and exposed to PDT.[17] In parallel, we also performed LegendPlex analysis following photoactivation of PS in spheroids. We found a notable upregulation of multiple chemokines, most of them known to be involved in immune cell migration and recruitment (figure 1F). While assay sensitivity limited detection at the highest PS concentration, the increase in all the chemokines (except one) was prevented with ferrostatin-1 (figure 1F). Further evidence of PDT’s potential to induce an anticancer immune response was obtained by documenting prophylactic vaccination in mice exposed to PDT-killed cancer cells, an approach regarded as the gold standard for demonstrating the ability of a therapeutic modality to induce ICD. Significant tumor growth delay and improved mouse survival were observed after challenging subcutaneously vaccinated mice with intraperitoneal (i.p.) injections of live cancer cells (figure 1G,H).

PDT-induced ferroptosis reduces spheroid outgrowth while increasing central cell death

Since the effects of bona fide ferroptosis inducers were reported to be poorly immunogenic,[27] we next compared the fate of spheroids exposed to either PDT or RSL3, a well-known ferroptosis inducer. We first validated the capacity of both strategies to induce lipid peroxidation through the detection of Bodipy 581/591 C11 green fluorescent signal (online supplemental figure 2A,B). A net difference was, however, observed in the spheroid growth with PDT exerting a rapid and profound increase in cytotoxicity together with a reduction in the spheroid volume whereas RSL3 cytotoxic effects were less pronounced and developed slower (figure 2A,B). We then compared the capacity of photoactivated PS and RSL3 to induce cell death in 3D spheroids by evaluating the distribution of propidium-iodide labeling across the cell layers (figure 2C,D). This led us to reveal that as soon as 6 hours post-PDT administration (figure 2C and online supplemental movie 1A,B), the external diameter of the spheroid was dose-dependently reduced (figure 2E for quantification) while the internal dead cell core was increased (figure 2F for quantification). The latter was determined based on the central area of propidium iodide exclusion, a paradoxical but common observation in spheroids thought to result from chromatin condensation and/or fragmentation and further leakage of damaged nuclear contents (see figure 2C). Both the PDT-induced reduction in spheroid size and expansion of the central dead cell area were prevented by ferroptosis inhibitor ferrostatin-1 (figure 2C,E,F and online supplemental movie 1C). By contrast, ferroptosis inducer RSL3 reduced the spheroid area to a much lesser extent and failed to increase the death cell core (figure 2D–F for quantification). Rapid PDT-induced inhibition of 3D spheroid growth and the progressive detachment of dead cancer cells were confirmed in phase contrast pictures depicting spheroids exposed to increasing doses of PS (vs RSL3 exposure) (online supplemental figure 2C). Interestingly, spheroid staining with the hypoxia marker pimonidazole led us to identify the central hypoxic core of the spheroid as the preferred location where PDT-induced cell death is initiated within the first few hours post-photoactivation; this is particularly visible at low PS dosage (30 nM OR141) (online supplemental figure 2D). At the higher doses, PI staining appeared excluded from the central core of the spheroids (as in figure 2C) and expanded over the hypoxic zone, progressively reaching the more external layers of the entire spheroid (online supplemental figure 2D). Altogether these results indicate that even if ferroptosis represents the major mode of cell death triggered by PDT, a non-canonical cell death mode leads to the preferred induction of cytotoxicity in the depth of 3D spheroids.

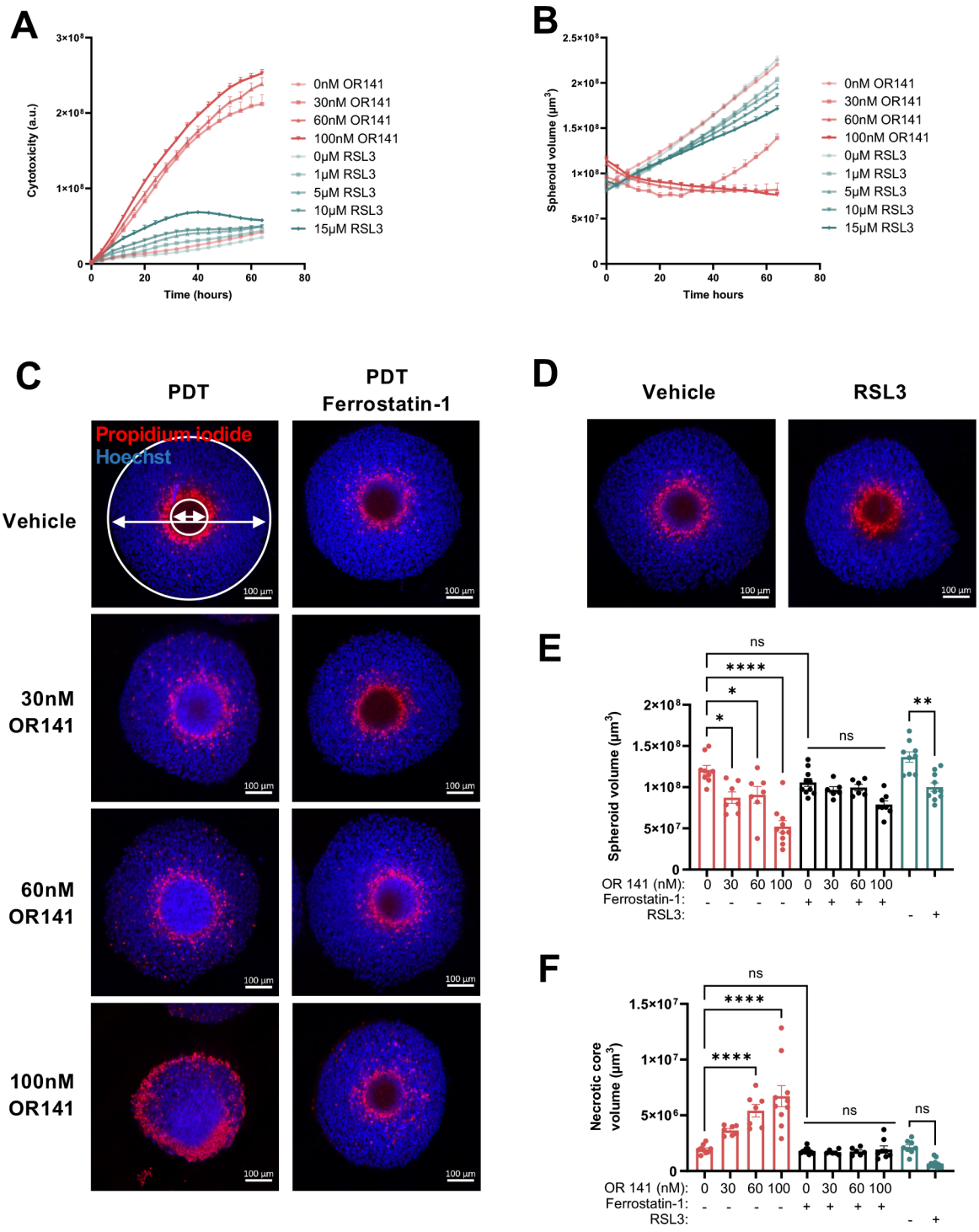

Figure 2 PDT exhibits distinct cell death kinetics and potency compared with the ferroptosis inducer RSL3. (A, B) CT26 three-dimensional (3D) spheroids were exposed to PS OR141 before 90 min LED light irradiation or to the ferroptosis inducer RSL3. (A) Cytotoxicity (cytotox green dye, Incucyte) and (B) growth (spheroid volume) (B) were followed over time. (C–F) CT26 3D spheroids were pretreated with 10 µM ferrostatin-1 and incubated 48 hours later with PS OR141 in the dark for 4 hours, followed by a washing step. Photoactivation was performed using an LED light source for 90 min and incubation was continued after the renewal of ferrostatin-1. A similar protocol was applied for RSL3 treatment with 48 hours pretreatment and renewal for final incubation. Representative light sheet microscopy pictures depicting propidium iodide-positive dead cells (red) and counterstained nuclei (blue) 6 hours after (C) PDT or (D) 5 µM RSL3 treatment. Scale bar: 100 µm. Quantification of (E) spheroid volumes (µm^3) and (F) necrotic core volume (µm^3) determined using Zen software (see white arrows in the top left panels). Data are plotted as the means±SEM (*p≤0.05; **p≤0.01; ****p≤0.0001; ns, p>0.05) from 3 independent experiments performed with ≥3 technical replicates; when spheroids are involved, minimum of 6 spheroids were pooled together per condition. Significance was determined by one-way ANOVA with Tukey's multiple comparison test. ANOVA, analysis of variance; ns, noi significant; PDT, photodynamic therapy.

PDT promotes the recruitment of iDCs in 3D spheroids and an increase in their cell volume

To evaluate the response of exogenous iDCs facing PDT-induced cell death, we first tracked their fate in 3D spheroids previously exposed or not to photoactivated PS OR141 (figure 3A). The resulting heterotypic 3D spheroids revealed a PS dose-dependent infiltration of $CD11c^+$ cells as determined in equatorial sections of 3D spheroids (figure 3B,D) whole spheroids analyzed using light sheet microscopy (LSM) (figure 3C,F for quantification; see also online supplemental movie 2A–C). Of note, the polarization of the entry of iDCs into spheroids corresponds to the bottom of the well where iDCs accumulate to a larger extent on addition in the culture wells. PDT induced a parallel reduction in spheroid size (figure 3B,C,G for quantification, also online supplemental movie 2C). Interestingly, LSM-based 3D cell reconstruction modeling strongly suggested that the enhanced DC infiltration was associated with an increase in DC volume (ie, DC size), indicating a progression toward a matured state (figure 3C and online supplemental movie 2C). Both iDC infiltration and reduction in spheroid size were prevented in the presence of ferrostatin-1 (figure 3B,F,G, online supplemental movie 2D). Interestingly, ferroptosis inducer RSL3 failed to induce such increased DC infiltration (figure 3D–F). We further validated by flow cytometry the PDT-triggered increased infiltration of $CD11c^+$ cells inside 3D spheroids, and the failure of RSL3 to do so (figure 3H and online supplemental figure 3A for gating strategy). Flow cytometry allowed us to confirm that the volume of $CD11c^+$ cells dose-dependently increased on exposure to activated PS OR141 (figure 3I), together with a significant increase in the number of MHCI-positive and MHCII-positive $CD11c^+$ cells in PDT-exposed spheroids (figure 3J,K). The expression level of costimulatory molecules CD40, CD80, CD86 and CCR7 was, however, not increased in $CD11c^+$ $MHCII^+$ cells 48 hours after spheroid infiltration, nor was the relative number of DCs positive for these markers at that time (online supplemental figure 3B–E). The need to pool approximately 20 spheroids per condition to extract DCs limited the ability to conduct extensive time course studies to identify a more optimal detection window using flow cytometry. Finally, it is worth to mention that independently of PDT exposure, ferroptosis inhibitor ferrostatin-1 showed a small increase in the expression in maturation markers (online supplemental figure 3B–E and figure 3J,K) that was, however, not associated with an increase in DC volume (figure 3I). Altogether, these data indicate that PDT-induced cell death in spheroids (but not exposure to ferroptosis inducer RSL3) drives a major recruitment of DCs, along with an increase in cell volume and the absolute numbers of $MHCI^+$ and $MHCII^+$ $CD11c^+$ cells, suggesting an enhanced capacity of DCs to capture and present antigens.

PDT promotes DC-mediated activation of $CD4^+$ and $CD8^+$ T cells and associated cytotoxic effects in 3D spheroids

We next evaluated whether PDT-dependent increase in infiltration and DC volume supported an increased capacity of T cell activation despite a mitigated stimulation of costimulatory molecules. For this purpose, we added naive T cells ($CD62L^+$ $CD44^-$ $CD25^-$ $CD3^+$) 48 hours after iDCs transfer to PDT-exposed spheroids (figure 4A and online supplemental figure 4A for gating strategy). After 6 days of coincubation, a significant T cell-dependent reduction in spheroid growth was observed in a PS dose-dependent manner in the experimental set-up where DCs were present (see phase contrast pictures in figure 4B at 100 nM of photoactived PS and quantification in figure 4C). Note that when PDT alone was used, spheroids had the time to regrow after 6 days, masking the cytotoxic effects observed at earlier timing in figures 1–3). Propidium iodide staining further confirmed T cell-mediated cytotoxic effects consecutive to PDT/iDC administration (see IF pictures in figure 4B). The degeneration of 3D spheroids was such that the dead cell core was sometimes expelled due to spheroid loss of integrity (online supplemental figure 4B) giving rise to PI labeling covering most of the remaining spheroids (figure 4B, middle panel) or exhibiting an asymmetrical distribution (online supplemental figure 4B). Interestingly, T cell-mediated cytotoxic effects were not observed in the presence of ferrostatin-1 (figure 4B,C) and could not be recapitulated with ferroptosis inducer RSL3 (figure 4D). Evidence for T cell activation was further obtained by flow cytometry identifying an increase in the $CD62L^-$ $CD44^+$ and $CD69^+$ phenotype within both $CD8^+$ (figure 4E,G) and $CD4^+$ T cells (figure 4F,H) in the experimental set-up including iDC addition on PDT-exposed spheroids (see also online supplemental figure 4C,D for quantification). Here again, T cell response was blunted when ferrostatin was used during the PDT prechallenge (figure 4E–H) but could not be recapitulated by ferroptosis inducer RSL3 (online supplemental figure 4E–G).

Combining iDC vaccination with in situ endoscope light-induced PDT achieves a robust immune memory response against peritoneal carcinomatosis

To gauge the applicability of the strategy in vivo, we next set up a model of in situ PDT administration using an endoscope LED white light to photoactivate OR141 within the inflated mouse peritoneal cavity (figure 5A). Peritoneal carcinomatosis induced by i.p. injection of luciferase-expressing AB1 cancer cells was used as an orthotopic tumor model in immunocompetent mice and adoptive transfer of iDCs was consecutively carried out through i.p. injection post-PDT administration. It is worth mentioning that for these in vivo experiments we opted to use AB1 mesothelioma cells instead of mesothelioma AB12 and colon CT26 cancer cells used above. This decision was influenced by the aggressive nature of CT26 tumors, which often reached the ethical endpoint by days 7–10 (ie, before the immune response could develop)

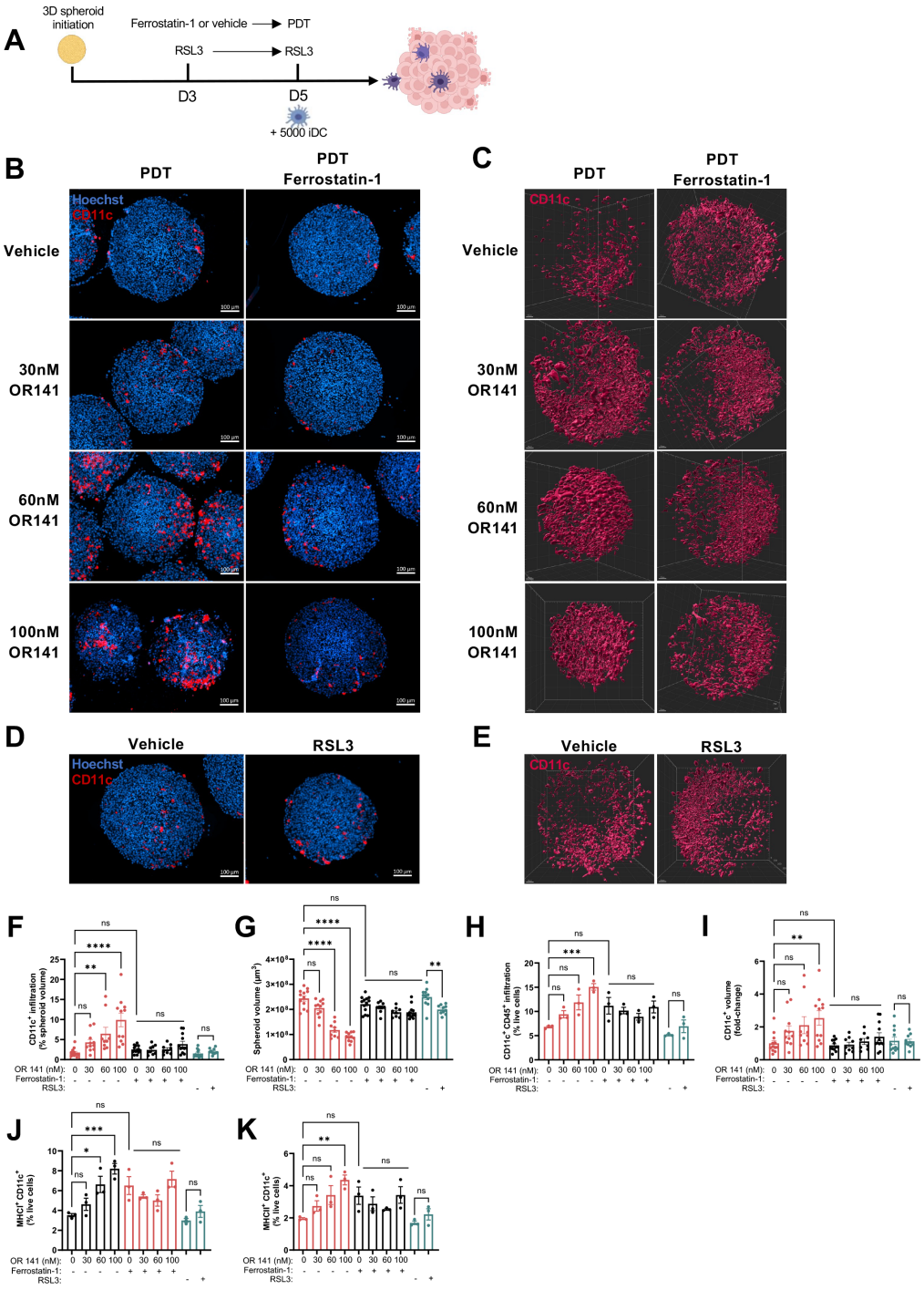

Figure 3 PDT-induced ferroptosis promotes iDC infiltration in three-dimensional (3D) spheroids together with an increase in MHCI and MHCII expression. (A) Protocol of iDC transfer to CT26 spheroids prechallenged with photoactivated OR141 or RSL3. CT26 3D spheroids were pretreated with 10 µM ferrostatin-1 and incubated 48 hours later with PS OR141 in the dark for 4 hours, followed by a washing step. Photoactivation was performed using an LED light source for 90 min and incubation was continued after the renewal of ferrostatin-1. A similar protocol was applied for RSL3 treatment with 48 hours pretreatment and renewal for final incubation. Exogenous iDCs (5×10^3 per spheroid) were added 48 hours post-PDT or after the last RSL3 addition. (B, D) Representative IF pictures depicting the extent of $CD11c^+$ cell infiltration after spheroid exposition to (B) PDT or (D) 5 µM RSL3. Scale bar: 100 µm. (C, E) Representative modeling of $CD11c^+$ cell infiltration (red) derived from light sheet microscopy-based reconstruction (Imaris program). Scale bar: 50 µm. (F) Quantification of wholemount IF-based infiltrated $CD11c^+$ cells and (G) impact on spheroid growth for the indicated conditions. (H) Flow cytometry-based quantification of infiltrated $CD11c^+$ cells and associated changes in (I) iDC volume, (J) MHCI and (K) MHCII expression. Data are plotted as the means±SEM (*p≤0.05; **p≤0.01; ***p≤0.001; ****p≤0.0001; ns, p>0.05) from 3 independent experiments performed with ≥3 technical replicates (minimum of 6 spheroids were pooled together per condition). Significance was determined by one-way ANOVA with Tukey's multiple comparison test. ANOVA, analysis of variance; iDC, immature dendritic cell; ns, not significant; PDT, photodynamic therapy.

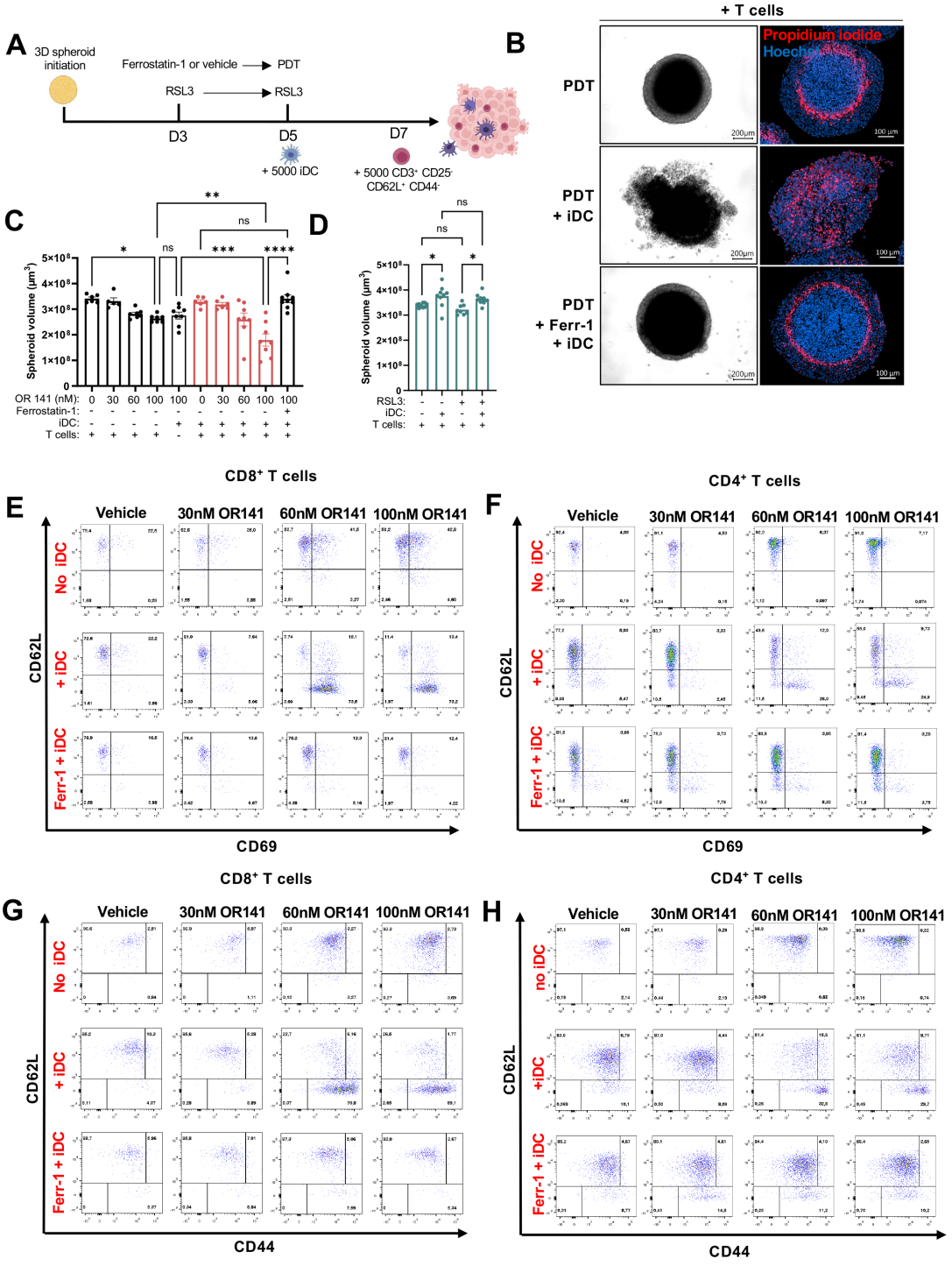

Figure 4 PDT promotes DC-mediated T cell response against three-dimensional (3D) spheroids. (A) Protocol of T cell transfer to CT26 spheroids primed by iDCs. CT26 3D spheroids were pretreated with 10 µM ferrostatin-1 and incubated 48 hours later with PS OR141 in the dark for 4 hours, followed by a washing step. Photoactivation was performed using an LED light source for 90 min and incubation was continued after the renewal of ferrostatin-1. A similar protocol was applied for RSL3 treatment with 48 hours pretreatment and renewal for final incubation. Exogenous iDCs (5×10^3 per spheroid) were added 48 hours post-PDT or after the last RSL3 addition, followed 48 hours later by addition of $CD62L^+$ $CD44^-$ $CD25^-$ $CD3^+$ lymphocytes (5×10^3 per spheroid); cytotoxic activity was analyzed 6 days later. (B) Representative phase-contrast (left panel, scale bar: 200 µm) and fluorescence pictures depicting propidium iodide positive (red) signal (right panel, scale bar: 100 µm) from CT26 spheroids treated as indicated, and (C) associated changes in spheroid volume (μm^3). (D) Lack of T cell-induced DC-mediated cytotoxic effects when RSL3 is used instead of PDT. (E–H) Flow cytometry-based phenotyping of $CD8^+$ (E, G) and $CD4^+$ (F, H) T cells using CD44, CD62L and CD69 markers from 3D spheroids treated as indicated. Data are plotted as the means±SEM (*p≤0.05; ** p≤0.01; ***p≤0.001; ****p≤0.0001; ns, p>0.05) from 3 independent experiments performed with ≥3 technical replicates (minimum of 6 spheroids were pooled together per condition). Significance was determined by one-way ANOVA with Tukey's multiple comparison test. ANOVA, analysis of variance; DC, dendritic cell; ns, not significant; PS, photosensitizer.

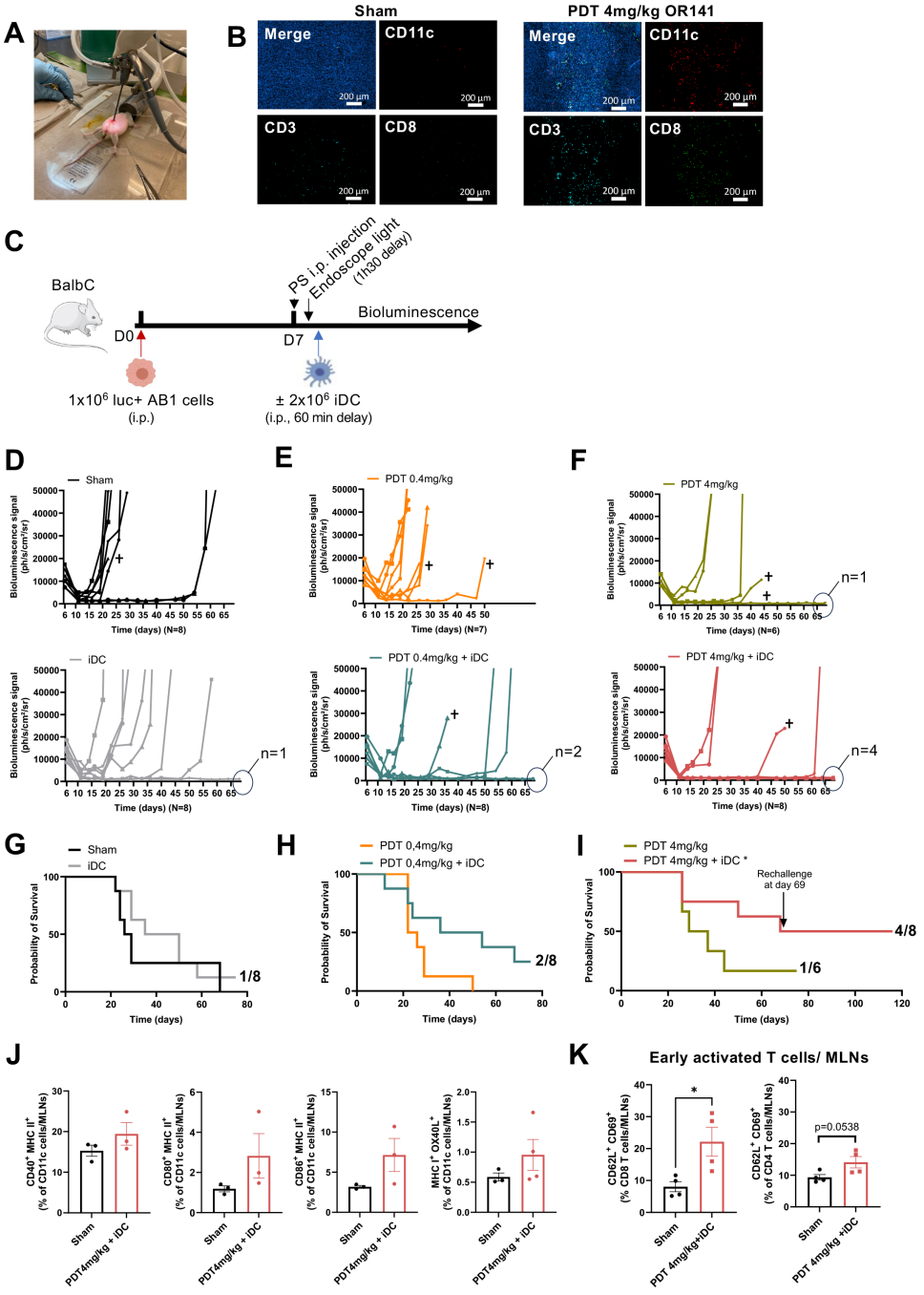

Figure 5 Laparoscopic PDT administration promotes iDC-based (memory) immune response against peritoneal tumors. Balb/CByJ mice were i.p. injected with 1×10^6 luciferase-positive AB1 tumor cells and exposed 7 days later to PDT. PS-OR141 (0.4 or 4 mg/kg) was injected i.p. 90 min before laparoscopy and photo-activated for 15 min on endoscopal light exposure; sham animals were used as controls. (A) Experimental set-up depicting laparoscopy procedure to introduce the endoscope LED light source in the inflated peritoneal cavity. (B) Representative multiplex immunofluorescence pictures depicting immune cell infiltration ($CD11c^+$ cells in red, $CD3^+$ T cells light blue and $CD8^+$ T cells in green) 6 days post in situ PDT. Scale bar: 200 µm. (C) Protocol of in situ PDT-based iDC vaccination against mouse peritoneal tumors. iDCs (2×10^6) were injected i.p. 60 min after in situ PDT. (D–F) Tumor burden monitored by bioluminescence (expressed as photons/s/cm^2/sr) and (G–I) corresponding survival curves. n=6–8 mice per group. Significance was determined by comparing curves presented in G–I with log-rank (Mantel-Cox) test (*p≤0.05). Experimental endpoint was determined when mice reached the ethical limits (ie, bioluminescence signal over 50,000 ph/s/cm^2/sr or euthanasia (†) on major ascite accumulation). In (I), arrow at day 69 indicates rechallenge by i.p. injection of 1×10^6 luciferase-positive AB1 tumor cells. (J, K) Immune cell activation analysis carried out by flow cytometry from mesenteric lymph nodes collected 10 days after treatment. Bar graphs represent (J) $CD40^+$, $CD80^+$, $CD86^+$ $MHCII^+$ and $OX40L^+$ $MHCI^+$ $CD11^+$ cells and (K) $CD62L^+$ $CD69^+$ early activated $CD8^+$ and $CD4^+$ T cells in PDT 4 mg/kg+iDC experimental condition (vs sham mice). Data are plotted as the means±SEM (*p≤0.05; ns, p>0.05) from 3 to 4 mice per group. Significance was determined by Student's t-test. iDC, immature dendritic cell; i.p., intraperitoneal; MLN, mesenteric lymph nodes; PDT, photodynamic therapy.

and at the opposite, by the slow growth of AB12 tumors leading to greater variability from mouse to mouse. AB1 cells were transduced with a luciferase-expressing vector to track the development of peritoneal carcinomatosis using in vivo detection of bioluminescence after luciferin administration (online supplemental figure 5A). Also, in a pilot study, we found that photoactivation of 40 mg/kg OR141 gave rise to lethal gastrointestinal toxicity in half of the mice whereas mice treated with 4 mg/kg OR141 dosage fully recovered from the procedure. As a proof of principle of the capacity of PDT alone to affect peritoneal carcinomatosis and induce ICD, we performed histological analysis of tumor samples collected 6 days after in vivo PDT. HE staining revealed extensive hypereosinophilic regions (online supplemental figure 5B) in comparison to peritoneal tumors from sham-operated mice, indicating extensive cellular damage resulting from PDT administration. Furthermore, hypereosinophilic areas were infiltrated by native T cells (online supplemental figure 5B). Multiplex immunohistofluorescence further confirmed an enhanced immune infiltration, demonstrating increases in both native CD11c$^+$ DCs, and CD3$^+$ and CD8$^+$ T cells in PDT-treated tumors, while these immune populations were largely absent in tumors from sham mice (figure 5B). We next examined the effects of this PS dosage and a yet smaller OR141 concentration (0.4 mg/kg) on the capacity of iDCs to influence tumor growth and mouse survival (see protocol in figure 5C). Follow-up of tumor growth revealed that iDCs alone delayed tumor growth (figure 5D) and that the combination with a PDT prechallenge further increased this delay and even completely prevented tumor regrowth in some mice (figure 5E,F) without signs of gross toxicity or weight loss (online supplemental figure 5C). Mouse survival was eventually not influenced by iDC transfer alone (figure 5G), while the combination of PDT and iDC transfer significantly increased mouse survival (ie, 25% and 50% mice still alive at day 80 in response to 0.4 and 4 mg/kg OR141, respectively) (figure 5H,I and online supplemental figure 5D for complete curve overlapping). In the latter condition, rechallenge with i.p. injection of cancer cells at day 69 did not give rise to detectable tumors (figure 5I). Absence of relapse was confirmed up to day 130, confirming a strong anticancer memory immune response. In a parallel experiment, we also documented that iDC administration in mice bearing larger tumors (PDT administered at day 15 instead of day 7) also led to tumor growth delay and mouse survival (ie, 20% mice) (online supplemental figure 5E,F).

To further characterize the PDT-induced immune remodeling, we collected mesenteric lymph nodes (MLNs) and spleens (10 days after treatment initiation) to evaluate DC maturation and T cell activation. In the MLNs from PDT/iDC-treated mice, we detected a consistent increase in the frequency of mature CD40$^+$, CD80$^+$, CD86$^+$ MHCII$^+$ DCs (figure 5J), together with a significant increase in CCR7$^+$ MHCII$^+$ DCs in the spleen (online supplemental figure 5G). This was accompanied by a significant rise in early-activated CD62L$^+$ CD69$^+$ CD8$^+$ (and CD4$^+$) T cells within MLNs (figure 5K), suggesting that matured DCs effectively induced T cell activation. Moreover, a trend toward activated CD62L$^-$ CD69$^+$ CD8$^+$ T cells was observed in both the spleen and MLNs (online supplemental figure 5H) as well as a significant increase in memory CD62L$^+$ CD44$^+$ CD8$^+$ and CD4$^+$ T cells in the spleen of PDT-iDC treated mice (online supplemental figure 5I). Notably, in two mice which had to be euthanized because of reaching the ethical limit point fixed in our protocol, we also found a marked increase in the infiltration of CD8 $^+$ T cells in the PDT/iDC condition (online supplemental figure 5J), among which a large population was CD39$^+$ supporting prior TA stimulation (online supplemental figure 5K).

Finally, we performed CD4 and CD8 T cell depletion experiments to assess whether the antitumor effects induced by PDT are mediated by T cells (online supplemental figure 5L–O). We confirmed CD4 and CD8 depletion after administration of blocking antibodies (online supplemental figure 5M). We found that the beneficial effects of PDT/iDCs combinatory treatment were lost when CD8 T cells (but not CD4 T cells) were depleted as documented by in vivo bioluminescence measurements of tumor burden (online supplemental figure 5N). Mouse survival was consecutively reduced on CD8 T cell depletion (online supplemental figure 5O).

iDC vaccination combined with in situ PDT enhances T cell proliferation and cytolytic activity

Splenocytes of surviving mice were collected at day 130 and exposed in vitro to AB1 spheroids in different ratios of effector to target cells (1:1; 4:1; 16:1) (figure 6A); note that these ratios overestimate the proportion of immune cells since they were calculated based on the amounts of cancer cells used to initiate the spheroids (which is largely inferior to the number of cancer cells in aged spheroids). After 7 days of coincubation, splenocytes from vaccinated mice (but not from control mice) led to significant growth inhibitory effects (4:1 ratio, see figure 6B) and ended up completely dismantling luc$^+$ AB1 spheroids (figure 6C); a trend toward growth inhibitory effect was observed at 1:1 ratio and a yet more pronounced response was obtained at the 16:1 ratio (online supplemental figure 6A). Moreover, a significant secretion of INF-γ was detected in the supernatant of spheroids exposed to splenocytes from vaccinated mice (ratio 4:1, figure 6D), confirming a strong PDT-induced anticancer immune response. These effects were confirmed using 2D co-cultures of luc$^+$ AB1 cells with vaccinated mouse splenocytes that revealed an enhanced CD8$^+$ T cell proliferation (4:1 ratio, figure 6E) and cytotoxicity (online supplemental figure 6B). These effects were further exacerbated at 16:1 ratio and already detectable in some replicates at an effector to target cell ratio 1:1 (online supplemental figure 6C). Finally, since luciferase expression itself could account for the observed immunogenic response, we also used non-luciferase but Nuclight transduced AB1 cancer cells to

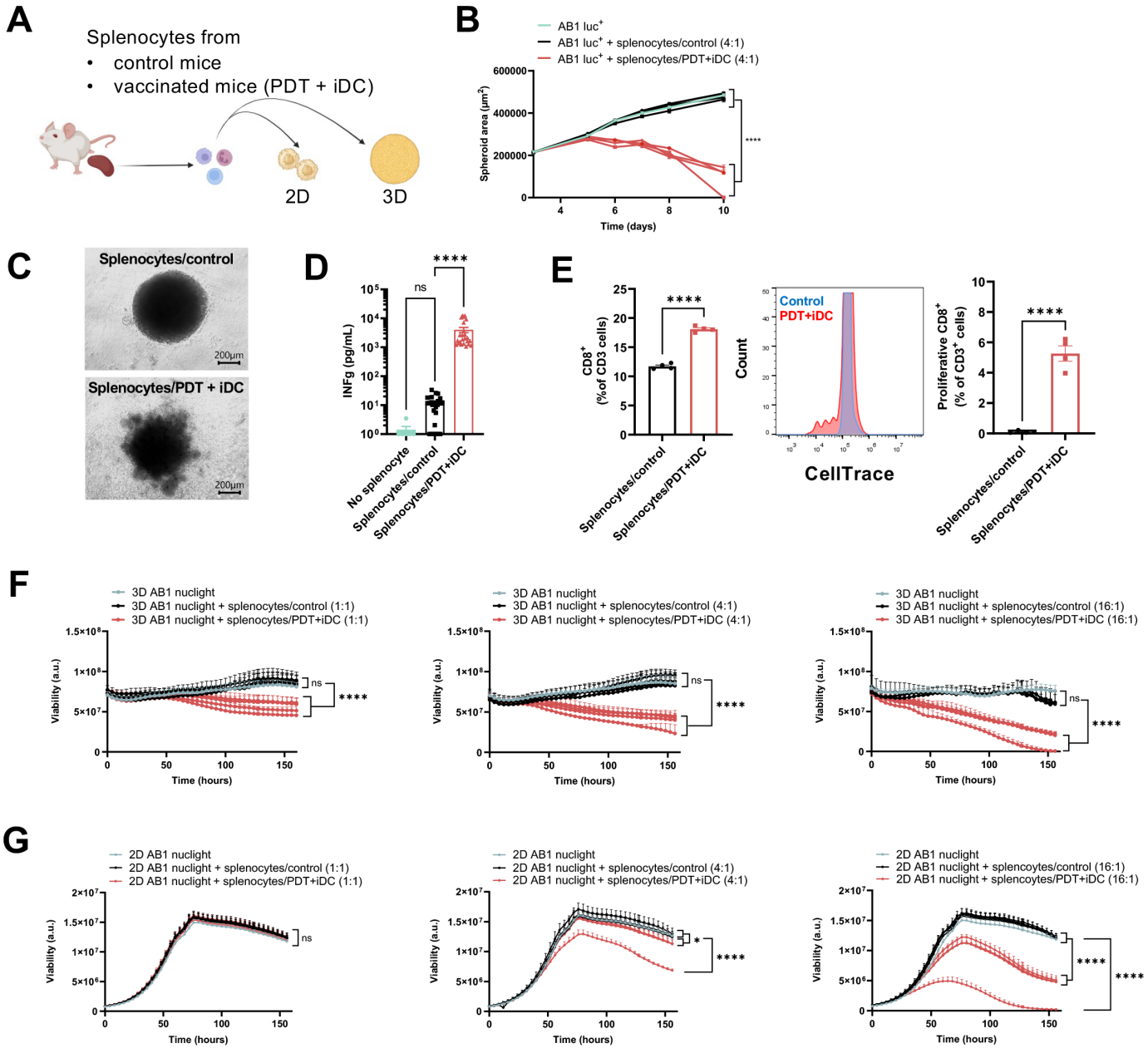

Figure 6 PDT combined with adoptive transfer of iDC induces ex vivo immune memory response. (A) Splenocytes were collected from vaccinated (surviving at day 130) or naive mice and exposed to AB1 cell monolayers (3×10^3 cells plated 24 hours before) or spheroids (5×10^3 cells plated 3 days before) at increasing effector to target ratios (ie, 1:1, 4:1 or 16:1, determined on the basis of cancer cell numbers at the time of plating). Immune memory response was evaluated using luc$^+$ AB1 spheroids co-cultured for 7 days (B–D) or luc$^+$ AB1 two-dimensional (2D) cell monolayers co-cultured for 3 days (E). (B) T cell-induced reduction in spheroid size, (C) representative pictures of cytotoxic effects at day 10 (scale bar: 200 µm) and (D) INFg-secretion in the spheroid supernatant assessed by ELISA at ratio effectors to targets 4:1. (E) Relative amount (left panel) and proliferation (middle and right panels) of CD8$^+$ T cells after exposure to AB1 2D cell monolayers (ratio 4:1). (F, G) Immune memory response was also evaluated by measuring viability signal (ie, gain or loss of nuclight signal over time, Incucyte) on exposure of luciferase-negative cancer cells cultured as spheroids (F) or monolayers (G) to splenocytes at the indicated effectors to target ratios. Data are plotted as the means±SEM (*p≤0.05; ****p≤0.0001; ns, p>0.05) from 4 independent splenocyte collections from mice with ≥3 technical replicates; when spheroids are involved, minimum of 6 spheroids were pooled per condition. Significance was determined by one-way ANOVA with Tukey's multiple comparison test. ANOVA, analysis of variance; iDC, immature dendritic cell; PDT, photodynamic therapy.

evaluate the strict contribution of endogenous TAs to the T cell response. For every ratio of effector to target cells, cell viability was reduced in 3D heterotypic spheroids (figure 6F). Surprisingly, 3D spheroids appear more sensitive than 2D cancer cells to the immune rechallenge (figure 6G), suggesting that microenvironment-related TAs (only present in 3D cultures) also participate to the response.

DISCUSSION

The main finding of this study is the demonstration that in situ PDT administration in the peritoneal cavity has the capacity to prime the tumor microenvironment, enabling iDCs to capture TAs and mount a potent T cell-based immune response. The potential for clinical application is major because there is today an unmet medical need for the treatment of peritoneal tumors or metastases, which severely impact patient outcomes. Additionally, the strategy is based on the use of a conventional tool, namely the light of an endoscope, and iDCs that do not require sophisticated bioengineering. Mechanistically, two critical factors driving the successful PDT-triggered iDC-based immune response were identified.

First, the reversal of the PDT-induced immune response by a ferroptosis inhibitor but the inability of a genuine ferroptosis inducer like RSL3 to replicate this effect, indicate that canonical ferroptotic cell death is necessary but not sufficient to support these effects. The overcoming of the effects of ferrostatin-1 at high PS dosage and the development of a PI-negative dead cell core within PDT-exposed 3D spheroids (a phenomenon not seen with RSL3) imply that PDT-induced cytotoxicity arises from intricate cell death processes. In earlier work, we documented that the strong pro-oxidant effects of OR141, the PS employed in this study, prompted the formation of high molecular weight complexes of multimeric proteins, partly through deubiquitinase inactivation, leading to detrimental ER stress (even in the presence of minimal amounts of O_2).[18] This aligns with the current observation of a preferred killing of hypoxic cancer cells located in the depth of spheroids and which are known to already harbor heightened ER stress levels. Also, contrary to superficial cell layers of 3D tumor spheroids, we previously showed that hypoxic/acidic cells were more prone to undergo ferroptosis because of an increased tropism for fatty acids (FA) including polyunsaturated FA that are the main targets for peroxidation.[32] Collectively, these findings suggest that while ferroptosis is essential for bolstering PDT's immunostimulatory effects, it does not explain the entire response. This echoes the ongoing debate about the immunogenic nature of ferroptosis when compared with other cell death types such as necroptosis.[27–29] In fact, our results can be paralleled with the coordinated interplay between the historical two forms of cell death (eg, apoptosis and necrosis) that can facilitate optimal cross-presentation of TAs.[2] Accordingly, apoptotic cell phagocytosis by iDCs yields antigenic peptides for MHCI and MHCII presentation, while exposure to necrotic tumor cells provides the necessary maturation signal.[11 33–36] Similarly, our data indicate that PDT by inducing ferroptosis in a non-canonical and/or non-exclusive manner (possibly due to spatiotemporal peculiarities) holds promise as a unique tool to induce an effective anticancer immune response. Interestingly, Shui *et al* using clinically approved PS hypericin, reported that PDT-induced cell death was independent of lipoxygenase and ACSL4, leading them to propose the term of liperoptosis to describe the ferroptosis-like mode of cell death induced by PDT.[37] The non-strict overlap between ferroptosis and PDT-induced cell death may well account for the remarkable immunostimulatory effects observed in our study.

Second, the favorable effects of PDT on the iDC-based immune response are largely attributable to their increased infiltration and enhanced endocytic capacity. This observation can be interpreted in light of PDT's direct cytotoxic effects, which lead to the release of a broad range of TAs alongside the generation of damage-associated molecular patterns (DAMPs). Indeed, we provide evidence that photoactivation of the PS used in this study (1) exerts direct cytotoxic effects, as confirmed by HE staining and supported by prior evidence of significant tumor growth delay when administered to immunocompromised mice[13] and (2) induces the release of various DAMPs, including HMGB1, calreticulin, Hsp90, Hsp70, and ATP (this study and[13]). This dual function is further suggested by our findings, which indicate that successful prophylactic vaccination with PDT-treated cancer cells may not only serve as a potential source of antigens but also contribute to creating an immune environment conducive to DC recruitment and enhanced antigen presentation. Additionally, the variety of chemokines we observed to be upregulated in response to PDT supports a model in which iDCs are attracted, followed by their acquisition of increased motility to reach secondary (or tertiary) lymphoid structures. This is consistent with our previous findings showing that in vitro PDT induces a stronger upregulation of CCR7 compared with LPS and enhances the migratory capacity of DCs, as demonstrated using the hind limb footpad assay.[17] Interestingly, DAMPs have the capacity to disrupt the canonical strategies used by cancer cells to maintain DC in their immature phenotype[38] but also to trigger the activation of CD4 T helper cells observed in the current study. This may actually support the memory effect observed in our model with the failure of mouse rechallenge with cancer cells to give rise to new tumors. Indeed, activation of $CD4^+$ T cells is known to ensure that after antigen recognition by $CD8^+$ T cells, CTLs will experience a long-term lifespan (instead of the activation-induced cell death characteristic of 'helpless' CTLs).[39] Such T-cell help is also likely to mitigate the lack of robust induction of costimulatory molecules and reduces the risk of tolerance induction associated with iDC administration. Finally, both the direct cell-killing effects and the creation of an immunogenic environment are likely to be intricately intertwined, as alterations in tumor 3D architecture ultimately ease the infiltration of recruited DC and T cells within PDT-exposed tumor tissues.

Collectively, our findings offer insights indicating that PDT administration may not only abrogate the necessity to stimulate iDCs with maturation cocktails

or to preload them with TAs. Interestingly, among the few trials evaluating the administration of iDCs in patients, DCs were either prechallenged with IFN-α to give rise to a phenotype endowed with a higher motility behavior while maintaining an elevated endocytotic capacity[40 41] or combined with radiotherapy to create an immunogenic environment.[42] Furthermore, in patients with advanced non-small cell lung carcinoma (NSCLC), the use of DC transduced with an adenoviral vector expressing secondary lymphoid tissue chemokine CCL21[43] aimed to take advantage of an increased DC attraction. Also, in these trials, intranodal (for lymphoma) or intratumoral (for NSCLC and melanoma) injections of DCs were used, highlighting the potential for spatially defining the interaction between DCs and cancer cells. Our study demonstrates that in situ PDT delivery may thus amalgamate critical aspects of these trials, including enhancing endocytotic and infiltration potential of iDCs while inducing a proimmunogenic environment confined to the peritoneal cavity. In situ PDT combined with iDC administration may also offer an advantage to currently explore alternative methods to deliver TAs to DCs in vivo.[2] Indeed, antigens can for instance be directly carried to DCs of patients with cancer on fusion with antibodies[44 45] or polypeptides that specifically target DC-specific receptors.[5] A notable advantage of PDT-induced cytotoxic effects is the access for iDCs to a broad spectrum of TAs, as opposed to relying on single or few epitopes when using in vivo targeted antigens or preloaded DCs. Interestingly, the acute cytotoxic effects of PDT may contribute to pulse DCs with a high dose of TAs, which is proposed to preferentially give rise to a sustained immunological memory[46]; some of these TAs may actually also be generated in response to the potent oxidizing stimulus induced by PDT.[47]

The fact that our study does not identify the nature of the antigens responsible for the antitumor T cell response may be seen as a limitation. However, several lines of evidence support the major role of tumor-specific CTLs in the observed immune response including (1) the lack of in vitro CD8 T cell activation and cytotoxic activity in the absence of iDC exposed to PDT-killed cancer cells (figure 4 and online supplemental figure 4), (2) the lack of an in vivo antitumor response when prechallenging mice with depleting anti-CD8 antibodies (online supplemental figure 5), (3) the detection of early activated CD8 T cells in MLNs of PDT/iDC-treated mice (figure 5) and (4) the ex vivo demonstration of an enhanced proliferation of $CD8^+$ T cells derived from vaccinated mice, along with a significant secretion of INF-γ and increased cytotoxicity toward spheroids (figure 6 and online supplemental figure 6). More generally, on PDT exposure, the release of a broad repertoire of anonymous antigens in a proimmunogenic environment may also enhance the activation of bystander T cells, thereby amplifying the overall immune response against tumors.

In conclusion, the combination of in situ PDT and iDC administration offers a multifaceted strategy to combat peritoneal tumors. To our knowledge, this study represents the first demonstration of using endoscopic light to locally induce an antitumoral immune response. This is all the more remarkable in the context of peritoneal carcinomatosis, where the current prognosis for the patient is most often unfavorable. Unlike conventional DC vaccines that target single TA, in situ PDT allows to set up iDC-based vaccines that leverage the entirety of each patient's tumor antigenic repertoire. Such strategy elicits robust and enduring antitumor immune responses, fostering memory immunity against cancer. Further optimization for clinical validation will include the selection of the most appropriate source of iDC to be combined with PDT and the possible gain in combining this strategy with immune checkpoint blockers.[4 48]

MATERIAL AND METHODS

2D cell culture

The Mouse AB1 (#10092305) and AB12 (#10092306) mesothelioma cell lines were purchased from ECACC and CT26 (CRL-2638) colorectal carcinoma cell line was acquired from ATCC. Cells were stored according to the supplier's instructions and used within 6 months after resuscitation of the frozen aliquots. Luciferase-expressing AB1 cell line (luc^+ AB1) was obtained by infection with firefly luciferase-encoding lentiviral particles (#LVP326, Amsbio), followed by selection with 2 µg/mL puromycin (#ant-pr-1, Invivogen), as described previously.[17] Fluorescent Nuclight red positive AB1 cells were generated on infection with Nuclight Red Lentivirus (EF1a, Puro) (#4476, Sartorius) and 5 µg/mL puromycin selection (#ant-pr-1, Invivogen). All cell lines were tested for mycoplasma contamination before use. Cells were maintained in RPMI 1640+GlutaMAX (#61870010, Thermo Fischer Scientific) supplemented with 10% heat-inactivated FBS (#F7524, lot: 0001650764, Sigma) and 1% penicillin-streptomycin (#15140122, Thermo Fischer Scientific) in a humidified atmosphere at 37°C and 5% CO_2.

Cell growth was monitored using a live-cell phase-contrast microscope (AxioVert25, Zeiss) and cell viability was assessed by using the PrestoBlue cell viability reagent (#A13262; Thermo Fisher Scientific) according to manufacturer's instructions, or quantified in real-time using fluorescent Nuclight red marker as detected by Incucyte device (SX5, Sartorius) with 10× objective and recommended software (total orange object integrated intensity, OCU×µm²/Image).

3D spheroid models

Spheroids were formed by seeding cancer cells in ultra-low attachment plates (#7007, Corning and #83.3925.400, Biofloat) with RPMI medium 1640 (#11835-030, Thermo Fischer Scientific) supplemented with 10% heat-inactivated FBS (#F7524, lot: 0001650764, Sigma), 2 mM L-glutamine (Thermo Fischer Scientific, #25030024), and

1% penicillin-streptomycin (Thermo Fischer Scientific, #15140122). 2000 AB12 or 5000 AB1 cells per well were seeded with 2% Cultrex basement membrane extract (#3532-005-02, Bio-Techne) while CT26 cells were seeded at a density of 500 cells per well without any matrix.

Spheroid growth was monitored using a live-cell phase-contrast microscope (AxioVert25, Zeiss) and spheroid aera was assessed using ImageFocusAlpha software (Euromex). Incycute device (SX5, Sartorius) was used to assess in real time spheroid growth and toxicity using Cytotox green dye (#4633, Sartotius). Spheroid images were acquired every 6 hours with the 10× objective, area and green fluorescence were measured with Incucyte softwares (largest brightfield object green integrated intensity (GCU×µm²)). Viability was quantified in real-time using fluorescent Nuclight red marker as detailed above.

Drug treatments and in vitro PDT

For experiments, 2D cell monolayers and 3D spheroids were treated 24 or 72 hours postseeding, respectively, with the following drugs: 10 µM ferrostatin-1 (#S7243, Selleckchem), 10 µM liproxstatin-1 (#S7699, Bioconnect), necrostatin-1 (#ab141053, Abcam, 20 µM for 2D and 30 µM for 3D), Zvad-fmk (#4026865, Bachem, 25 µM for 2D or 40 µM for 3D) or ferroptosis inducer RSL3 used as a positive control (5 µM for 3D). 48 hours after pretreatment, 2D cell cultures or 3D spheroids were incubated with the benzophenazine PS OR141 in the dark for 1 hour (2D) or 4 hours (3D) at the indicated concentrations, followed by washing. Photoactivation was performed using an LED light source (3.1 W, 6500 K, 230 lm, Refled ES50, Sylvania) for 60 min for 2D cultures or 90 min for 3D spheroids, respectively. Cell death inhibitors, where required, were maintained during and after the photoactivation period to ensure effective inhibition; RSL3 treatment of 3D tumor spheroids was renewed 48 hours after preincubation.

Mice

Female 6-week Balb/CByJ mice were purchased from Charles Rivers Laboratories.

Bone marrow-derived DCs

Bone marrow cells were extracted from the femurs and tibias of Balb/CByJ mice using previously described protocols.[49] After euthanizing the mice, bones were collected, sterilized for 5 min in 70% ethanol, and washed with PBS (Phosphate Buffered Saline). Both ends of the bones were sectioned using a scalpel, and the bone marrow was flushed using a 26G ½" syringe (#303800, BD Microlance) with RPMI 1640 Medium (#61870-010, Thermo Fischer Scientific) supplemented with 10% heat-inactivated FBS (#F7524, lot: 0001650764, Sigma) and 1% penicillin-streptomycin (#15140122, Thermo Fischer Scientific). Collected cells were centrifuged for 5 min at 500 g at 4°C. After red blood cell removal using eBioscience RBC Lysis Buffer (#00-4333-57, Thermo Fisher Scientific), cells were washed with PBS, centrifuged (5 min at 500×g) and cultured in RPMI 1640 Medium (#61870-010, Thermo Fisher Scientific) supplemented with 10% heat-inactivated FBS (#F7524, lot: 0001650764, Sigma) and 1% penicillin-streptomycin (#15140122, Thermo Fisher Scientific). Recombinant murine granulocyte-macrophage-colony-stimulating factor (20 ng/mL, #315-03, Peprotech,) and IL-4 (20 ng/mL, #214-14, Peprotech) were added to the medium as differentiation factors together with 50 µM β-mercaptoethanol as antioxidant.[50] Bone marrow-derived DCs (BMDCs) were seeded at a concentration of 800,000 cells/mL and maintained in an incubator with a humidified atmosphere at 37°C and 5% CO_2. After 3 days, half of the medium was removed and replaced with a double volume of fresh growth medium. On day 6, immature BMDCs were used in the described experiments.

Naïve T cells

Naive T cells were generated from mouse spleen extracts. The spleen was dissociated by mechanical pressure in ACK lysis buffer (#A1049201, Thermo Fischer Scientific) for 1 min. The lysis was stopped using cold RPMI media. The cell suspension was passed through a 40 µm cell strainer and centrifuged for 7 min at 300 g at 4°C. The pellet was washed two times in media and centrifuged. Cells were then counted and labeled with the CD3ε MicroBead Kit, mouse (#130-094-973, Miltenyi Biotec), as described by the manufacturer. At the end of the protocol, cells were labeled with anti-biotin microbeads and antibodies against APC anti-mouse CD3e (#553066, clone 145-2 C11, 1/100, BD Biosciences), BB515 Anti-Mouse CD25 (#564424, clone PC61, 1/100, BD Biosciences), PE-Cy7 Anti-Mouse CD44 (#560569, clone IM7, 1/100, BD Biosciences), and PE anti-mouse CD62L (#553151, clone MEL-14, 1/200, BD Biosciences) in the presence of purified rat anti-mouse CD16/CD32 (mouse BD Fc Block) (#553142, 1/200, BD Biosciences) for 15 min at 4°C. Cells were washed and centrifuged for 7 min (300 g) at 4°C before resuspension (1.25×10^8 cells in 500 µL buffer) before separation of CD3ε labeled positive cells on a MACS LS column (#130-042-401, Miltenyi). From the collected CD3ε positive cells, $CD62L^+$ $CD44^-$ $CD25^-$ $CD3^+$ naive T cells were sorted using a BD FACSAria III Cell Sorter (BD Biosciences).

Cell isolation

Single cell suspensions from 3D spheroids were obtained by enzymatic digestion with accutase incubation (#00-4555-56, Thermo Fischer Scientific) for 15 min under shaking at RT, combined with mechanical dissociation by pipetting up and down every 5 min.

Single-cell suspensions from tumors were obtained using the mouse tumor dissociation kit (Miltenyi Biotec, #130096730) in combination with the gentleMACS Octo Dissociator with heaters (Miltenyi Biotec). Briefly, tumor specimens were cut into 2–4 mm pieces using a scalpel and transferred to a gentleMACS tube containing the enzyme mix. Tissue dissociation was performed using

the program 37C_m_TDK_2, optimized for tough tumor tissues. Red blood cells were lysed using RBC lysis buffer (#00433357, Invitrogen), filtered on a 70 µm strainer, washed and centrifuged (5 min, 500 g) two times before analysis.

Splenocytes were generated from mouse spleen extracts. The spleen and the MLN were dissociated by mechanical pressure in ACK lysis buffer (#A1049201, Thermo Fischer Scientific) for 1 min, filtered on a 40 µm strainer, washed and centrifuged (7 min, 300 g) two times before analysis.

Flow cytometry analysis

For cell death staining, cells were incubated with 1 mg/mL propidium iodide (#P4170, Sigma-Aldrich) in PBS and directly analyzed by flow cytometry. To assess the type of cell death, a suspension of 10^5 cells/mL was incubated with FITC Annexin V (#556420, 1/200, BD Biosciences) and 7-AAD (#559925, 1/200, BD Biosciences) in 1x Annexin V Binding Buffer (#556454, BD Biosciences) for 18 min in the dark before acquisition with flow cytometer.

Lipid peroxidation was assessed as described before,[32] using a fluorescent lipid probe C11-BODIPY581/591 (4,4 -difluoro-5-(4-phenyl-1,3-butadienyl)-4bora-3a,4a-diaza-s-indacene-3-undecanoic acid, #D3861, Thermo Fisher Scientific). Briefly, after spheroid dissociation, single cells were incubated with 3 µM C11-BODIPY581/591 for 30 min at 37°C. Cells were then washed and red/green fluorescence levels were determined (red: λexc=485 nm, λem=520 nm; green: λexc=485 nm and λem=595 nm) using FACSCanto II flow cytometer with BD FACSDiva Software (BD Biosciences).

Phenotyping of DCs, T cells and splenocytes was carried out after a 20 min incubation at 4°C in the presence of purified rat anti-mouse CD16/CD32 (mouse BD Fc Block) (#553142, 1/200, BD Biosciences). The specific antibodies used to profile immune cells are listed below.

For DCs: PE/cyanine7 anti-mouse CD45 (#103113, clone 30-F11, 1/200, BioLegend), Brilliant Violet 785 anti-mouse CD11c (#117335, clone N418, 1/200, BioLegend), FITC anti-mouse I-A/I-E (#107605, clone M5/114.15.2, 1/200, BioLegend), PE anti-mouse CD40 (#124609, clone 3/23, 1/200, BioLegend), Brilliant Violet 421 anti-mouse CD86 (#105031, clone GL-1, 1/200, BioLegend), Brilliant Violet 605 anti-mouse CD197 (#120125, clone 4B12, 1/200, BioLegend), PE/Dazzle 594 anti-mouse CD80 (#104737, clone 16-10A1, 1/200, BioLegend). Live/dead exclusion was achieved by staining with a Zombie aqua fixable viability kit (#423101, 1/1000, BioLegend).

For T cells, the following antibodies were used: brilliant violet 510 anti-mouse CD45 (#103138, clone 30-F11, 1/200, BioLegend), APC anti-mouse CD3e (#553066, clone 145-2C11, 1/100, BD Biosciences), APC-Vio 770 anti-mouse CD8a REAfinity (#130-120-806, clone REA601, 1/500, Miltenyi Biotec), FITC anti-mouse CD69 antibody (#104505, clone H1.2F, 1/100, BioLegend), PE anti-mouse CD62L (#553151, clone MEL-14, 1/200, BD Biosciences), PE-Cy7 anti-mouse CD44 (#560569, clone IM7, 1/200, BD Biosciences). Live/dead exclusion was achieved using fixable violet dead cell stain kit (#L34955, 1/1000, Thermo Fisher Scientific).

For splenocytes, the following antibodies were used:: BV510 anti-CD45 (#103138, clone 30-F11, 1/200, BioLegend), APC anti-CD3 (#553066, clone 145-2C11, 1/100, BD Biosciences), PE anti-CD8 (#100708, clone 53-6.7, 1/250, BioLegend) and FITC anti-CD4 (#100405, clone GK1.5, 1/200, BioLegend), APC-Cy7 anti-CD19 (#152411, clone 1D3/CD19, 1/250, BioLegend) with live/dead exclusion was achieved using fixable violet dead cell stain kit (#L34955, 1/1000, Thermo Fisher Scientific).

For tumor reactive CD8 T cells, the following antibodies were used: BV510 anti-CD45 (#103138, clone 30-F11, 1/200, BioLegend), Pe-Cy7 anti-CD3 (#100220, clone 17A2, 1/250, BioLegend), PE anti-CD8 (#100708, clone 53–6.7, 1/250, BioLegend) and APC anti-CD39 (#143810, clone Duha59, 1/200, BioLegend) with live/dead exclusion was achieved using fixable violet dead cell stain kit (#L34955, 1/1000, Thermo Fisher Scientific).

To analyze proliferation, T cells were preincubated with CellTrace violet cell proliferation kit (#C34571, Invitrogen) according to manufacturer's instructions. Antibodies against PE anti-mouse CD3 REAfinity (#130-121-133, clone REA641, 1/250, Miltenyi Biotec) and FITC anti-mouse CD8a (#553031, clone 53-6.7, 1/150, BD Biosciences) were used for 20 min incubation at 4°C in the presence of purified rat anti-mouse CD16/CD32 (mouse BD Fc Block) (#553142, 1/200, BD Biosciences), in combination with eBioscience fixable viability dye eFluor 780 (#65-0865-14, 1/1000, Invitrogen) to exclude dead cells.

Experiments were performed on a FACSCanto II flow cytometer with BD FACSDiva Software (BD Biosciences), and a NovoCyte Quanteon Flow Cytometer Systems 4 Lasers with NovoExpress Software (Agilent) (only for DC maturation analysis). Data were analyzed using the FlowJo software (BD Biosciences) with a gating strategy excluding debris and doublet cells.

Immunofluorescence

To assess hypoxia, 3D tumor spheroids were treated with 1 µM pimonidazole (#N1165, Merck) for 24 hours prior to sample collection. For cell death staining, spheroids were incubated with 1 mg/mL propidium iodide (#P4170; Merck) for 15 min under continuous shaking to ensure even staining. Afterward, samples were washed and fixed overnight with 4% formaldehyde (#P0875, Carl ROTH), then incubated with 30% sucrose for 30 min and finally embedded in Neg-50 (#6502Y, Epredia), before being frozen in 2-methylbutanol cooled in liquid nitrogen and storage at −80°C. Frozen sections (5 µm) were permeabilized 10 min in PBS-triton 0.5% at RT and then blocked with PBS-triton 0.05% (PBST)- 5% BSA during 1 hour at RT, incubated overnight at 4°C with anti-pimonidazole primary antibody (#Pab2627, 1/400, Hyopxyprobe) or anti-CD11c primary antibody (#97585, 1/150, Cell Signaling) in PBST-1% BSA. Spheroid sections were then

incubated with Alexa Fluor Plus 488-conjugated anti-rabbit secondary antibodies (#A32790, 1/1000, Thermo Fisher Scientific) or Alexa Fluor Plus 555-conjugated anti-rabbit antibody secondary antibody (#A32794, 1/1000, ThermoFischer Scientific) for 1 hour and nuclei were counterstained with Hoechst 33 342 (#14533, Sigma). Slides were mounted with fluorescence mounting medium (#S3023, Dako), and images were acquired using Axioscan.z1 and visualized using ZEN Blue software (Zeiss). All the spheroid samples from the same experiment were imaged using the same experimental settings. Immunofluorescence images were analyzed with Zen Blue (Zeiss).

Wholemount immunofluorescence and 3D LSM

Dead cells were stained with 1 mg/mL propidium iodide (#P4170; Merck) for 15 min under shaking. Spheroids were fixed with 4% formaldehyde for 24 hours, blocked, and permeabilized at 4°C overnight in PBS-Triton X-100 0.5% containing 5% BSA. Whole spheroids were incubated with anti-CD11c primary antibody (#97585, 1/150, Cell Signaling) at 4°C for 5 days with shaking and then incubated with Alexa Fluor Plus 555-conjugated anti-rabbit antibody secondary antibody (#A32794, 1/500, ThermoFischer Scientific) and Hoechst33342 (#H3570, 1/5000, Invitrogen) in PBS-Triton X-100 0.05%–1% BSA at 4°C for 4 days with shaking. The antibody incubation was followed by 2 hours of 4% formaldehyde fixation and spheroid clearing with CUBIC 1 for 4 days and CUBIC 2 for 3 days. CUBIC1 and 2 were prepared according to the protocol described elsewhere.[51] Spheroids were mounted into 1% agarose in capillaries and visualized using a Lightsheet.z1 microscope (Zeiss). Immunofluorescence results were visualized using Zen Blue (Zeiss) or modelized with Imaris software (Bitplane), where specific object volumes (spheroids, DCs) were quantified. All the spheroid samples from the same experiment were imaged using the same experimental settings.

Multiplex immunofluorescence

Five µm FFPE sections of tumors were obtained by samples fixation in 4% formaldehyde (#P0875, Carl ROTH) for 48 hours, before paraffin impregnation with Tissue Tek VIP (Sakura) and paraffin inclusion with Tissue Tek TEC (Sakura).

Tyramide signal amplification modality was used, as described before,[52] starting with (1) deparaffinization (toluol and isopropanol); (2) endogenous peroxidase inactivation (3% H_2O_2 diluted in 100% isopropanol) and cycles for each antibody with following steps: (3) heat induced epitope retrieval (in citrate buffer pH 5,7), (4) blocking of aspecific antibody binding (5% BSA 0.1% Tween 20 (TBS-T)); (5) primary antibody incubation with anti-CD11c (1st position, #97585, 1/150, Cell Signaling), anti-CD8 (2nd, #98941, 1/200, Cell Signaling), anti-CD3 (3rd, #99 940T, 1/50, Cell Signaling), anti-CD45 (4th, #70257, 1/100, Cell Signaling) in 1%BSA TBS-T containing 0.01% sodium azide and 10% glycerol; (6) secondary antibody EnVision+anti-rabbit coupled to HRP (#K4003, Dako); and (7) incubation with fluorescent AF or CF conjugated tyramides (AF594: 1/100, #B40957, ThermoFischer Scientific; CF488: #92171, 1/1000, Biotium; CF555: #96021, 1/1000, Biotium; CF754: #96090, Biotium, respectively) diluted in 0.1 M borate, pH 7.8, 3M NaCl supplemented with 0.003% H_2O_2. After the cycles, nuclei were counterstained with Hoechst 33 342 (#14533, Sigma), and slides were mounted with fluorescence mounting medium (#S3023, Dako). Sections were scanned and acquired with an Axioscan.z1 (Zeiss) and visualized using ZEN Blue software (Zeiss). All the spheroid samples from the same experiment were imaged using the same experimental settings.

H&E staining

Five µm FFPE sections of tumors were obtained by samples fixation in 4% formaldehyde (#P0875, Carl ROTH) for 48 hours, before paraffin impregnation with Tissue Tek VIP (Sakura) and paraffin inclusion with Tissue Tek TEC (Sakura). Following deparaffinization in toluene and isopropanol, tumor sections were stained with Mayer's hematoxylin (#VWRK64040/1, VWR) for 10 min. The sections were then washed sequentially in tap and distilled water, followed by staining with 0.5% Eosin Y solution in water (#X883.2, Carl Roth) for 4 min. After additional washes in tap and distilled water, the slides were allowed to air dry. Finally, the stained slides were mounted using Sakura Tissue-Tek Film (Sakura).

In vivo prophylactic vaccination

A total of 10^7 luc^+ AB1 cells were killed in vitro via PDT using 100 nM of OR141 in a 100 mm dish containing 2.5 mL of PBS. Immediately after LED light irradiation, the dying cells were scraped from the dish and 250 µL (containing 1×10^6 cells) were subcutaneously injected into the left flank of 6-week-old Balb/CByJ mice. Control mice were injected with 250 µL PBS alone.

Seven days after vaccination, all mice were challenged with an i.p. injection of 1×10^6 luc^+ AB1 cells. Tumor growth was monitored three times per week by bioluminescence imaging: after i.p. injection of 4 mg Xenolight D-luciferin Potassium Salt (#122799, Perkin Elmer), bioluminescent signals (photons/s/cm^2/sr) were captured using the PhotonIMAGER system (Biospace Lab) and analyzed with M3Vision software (Biospace Lab). Mice were euthanized on reaching ethical endpoint criteria.

In vivo PDT procedure

Mice were i.p. injected with 1×10^6 luciferase-positive AB1 cells in 100 µL saline solution and tumor burden was followed three times a week by bioluminescence (ph/s/cm^2/sr) after i.p. injection of 4 mg Xenolight D-luciferin Potassium salt (#122799, Perkin Elmer) using a PhotonIMAGER (Biospace Lab). Pictures were analyzed with M3Vision software (BiospaceLab). On day 7 or 15, PDT was performed as followed: PS OR141 (0.4 or 4 mg/kg vs DMSO as vehicle) was administered i.p. and mice were

placed in the dark for 90 min before the PDT procedure. A pursing-string suture was performed in the middle of the abdomen to insert the endoscope airtightly. The Karl Storz-endosckope was equipped with a cold light source D Light P SCB (#201337, Karl Stozr, Xenon, 300 W, 6000 K), a camera system IMAGE1 S TM (# TC300 and # TH102, Karl Storz), an optic system (# STZ 64301AA, Hopkins), and a Vetpump 2 (#693216, Karl Storz) to inflate the peritoneal cavity for optimal light diffusion. Mice were light-exposed for 15 min, followed 1 hour later by i.p. injection of 2×10^6 iDC in saline solution. The experimental endpoint was determined when mice reached the ethical limit points.

In vivo T cell depletion

T cell depletion was performed as previously described,[53] using specific depleting or control (#400675, clone RTK4530, BioLegend) antibodies. Mice received an i.p. injection of 500 µg of monoclonal antibodies anti-CD4 (#100470, clone GK1.5, BioLegend) and anti-CD8 (#100776, clone 53-6.7, BioLegend), 1 day before in vivo PDT. This was followed by weekly doses of 250 µg anti-CD4 and 150 µg anti-CD8. The efficacy of T cell depletion was confirmed by flow cytometry 48 hours after the first depletion.

Western blotting

Spheroids were washed twice with PBS and lysed with Precellys (Bertin) with 1.4 mm zirconium oxide beads (#10402, Precellys) (3×30 s) in radioimmunoprecipitation assay buffer supplemented with 1% Protease Inhibitor Cocktail (#P8340, Sigma) and anti-foam (#A6457, Sigma). Protein concentration was determined using Pierce bicinchoninic acid-based assay protein assay (#23225, Thermo Scientific). Samples were then denatured (7 min, 95°C) in Laemmli buffer containing 100 mM dithiothreitol. Afterward, the samples (20 µg per well) were separated by SDS-PAGE (10% acrylamide/bis-acrylamide gels) and transferred to PVDF membranes. Membranes were then blocked with 5% skimmed milk in TBS-0.1%Tween 20 (TTBS) and subsequently immunoblotted overnight at 4°C with specific primary antibodies (MDA (#ab6463, Abcam, 1:1000), COX2 (#12282, Cell Signaling, 1:1000), HSP70 (#4872, Cell signaling, 1:1000) and beta-actin (#A5441, Sigma-Aldrich, 1:5000)). After several washes with TTBS, membranes were incubated for 1 hour at room temperature with horseradish peroxidase (HRP)-conjugated secondary antibodies (Jackson Immunoresearch), and chemiluminescence signals were detected using the ECL Western Blotting Detection Kit (# RPN2134, VWR) on X-ray films.

ATP assay

Extracellular ATP release from 3D spheroid cultures was quantified using the RealTime-Glo ATP Assay (#GA5010, Promega), following the manufacturer's instructions. Spheroids were exposed to PDT and subsequently incubated with the assay reagent at a 1:4 dilution. Luminescence was measured 30 min post-PDT using a SpectraMax i3x plate reader (Molecular Devices). Data are presented as fold change in luminescence relative to the untreated control condition.

Chemokine assay

Chemokine levels in the supernatants of spheroid cultures (in 50 µL volume) were quantified using the LEGENDplex Mouse Proinflammatory Chemokine Panel (13-plex) with V-bottom Plate (#740451, Biolegend), according to the manufacturer's instructions. The panel simultaneously measured CCL5 (RANTES), CCL20 (MIP-3α), CCL11 (Eotaxin-1), CCL17 (TARC), CXCL1 (KC), CCL2 (MCP-1), CXCL9 (MIG), CXCL10 (IP-10), CCL3 (MIP-1α), CCL4 (MIP-1β), CXCL13 (BLC), CXCL5 (LIX), and CCL22 (MDC). Bead-based immunoassays were analyzed using the NovoCyte Quanteon Flow Cytometer System (four lasers) with LEGENDplex Data Analysis Software Suite (Qognit).

IFN-γ assay

Interferon-γ in the supernatant was quantified with the mouse IFN-gamma DuoSet ELISA (#DY485, R&D Systems), according to manufacturer's instructions.

Statistical analysis

Data were expressed as mean±SEM of 3 independent experiments with ≥3 technical replicates, when spheroids are involved, minimum of 6 spheroids were pooled together per condition. Statistical analyses were performed through GraphPad Prism V.10 using Student's t-test, one-way ANOVA with Tukey's multiple comparison test, or with log-rank (Mantel-Cox) test when appropriate. Statistical significance is indicated in the figures as follows: *p≤0.05; **p≤0.01; ***p≤0.001; ****p≤0.0001, and ns, not significant when p>0.05.

Author affiliations
[1]Institut de Recherche Expérimentale et Clinique (IREC), Pole of Pharmacology and Therapeutics (FATH), Cancer Translational Research laboratory, UCLouvain, Brussels, Belgium
[2]IPHY Platform, Institut de Recherche Expérimentale et Clinique (IREC), UCLouvain, Brussels, Belgium
[3]CytoFlux-Flow Cytometry and Cell Sorting Platform, Institut de Recherche Expérimentale et Clinique (IREC), UCLouvain, Brussels, Belgium
[4]Imaging Platform 2IP, Institut de Recherche Expérimentale et Clinique (IREC), UCLouvain, Brussels, Belgium
[5]Walloon Excellence in Life Sciences and BIOtechnology (WELBIO), WEL Research Institute, Wavre, Belgium

X Charline Degavre @chadgvre

Acknowledgements We would like to acknowledge Ana Beloqui Garcia and Wunan Zhang for the access and training to the endoscope equipment, Aurélie Daumerie and Pierre Michel for their precious help for imaging experiments, Marie-Lucie Racu for histological interpretation, as well as Rachid El Kaddouri and Radu Bachmann for technical support for in vivo studies.

Contributors Conceptualization: CD and OF; Experimental work: CD, CG, HE, FL-M, AL and CF; Data analysis and interpretation: CD, AL and OF; Methodology: CD, AL, SI, KG, CF, HE, DB and CB; Writing: CD and OF; Funding and resources: OF; Supervision: OF. OF is the guarantor of the study.

Funding This work was supported by grants from the Fonds de la Recherche Scientifique (F.R.S.-FNRS, PDR T008719F and EOS 0002522F), WELBIO (Walloon

Excellence in Life Sciences and Biotechnology, X104022F), the (Belgian) Foundation against cancer (2020-074), and an Action de Recherche Concertée (ARC 19/24-096). OF is a Walloon Excellence in Life Sciences and Biotechnology (WELBIO) senior fellow and CD is a FRIA PhD student.

Competing interests None declared.

Patient consent for publication Not applicable.

Ethics approval Study protocols involving mice were approved by the ethic committee from UCLouvain (2020/UCL/MD/032) and were carried out according to national animal and European care regulations.

Provenance and peer review Not commissioned; externally peer reviewed.

Data availability statement Data are available on reasonable request.

ORCID iD

Olivier Feron http://orcid.org/0000-0001-5360-0286

REFERENCES

1 Cintolo JA, Datta J, Mathew SJ, *et al*. Dendritic cell-based vaccines: barriers and opportunities. *Future Oncol* 2012;8:1273–99.
2 Palucka K, Banchereau J. Cancer immunotherapy via dendritic cells. *Nat Rev Cancer* 2012;12:265–77.
3 Steinman RM. Dendritic Cells In Vivo: A Key Target for a New Vaccine Science. *Immunity* 2008;29:319–24.
4 Heras-Murillo I, Adán-Barrientos I, Galán M, *et al*. Dendritic cells as orchestrators of anticancer immunity and immunotherapy. *Nat Rev Clin Oncol* 2024;21:257–77.
5 Garg AD, Vara Perez M, Schaaf M, *et al*. Trial watch: Dendritic cell-based anticancer immunotherapy. *Oncoimmunology* 2017;6:e1328341.
6 Anguille S, Smits EL, Lion E, *et al*. Clinical use of dendritic cells for cancer therapy. *Lancet Oncol* 2014;15:e257–67.
7 Kantoff PW, Higano CS, Shore ND, *et al*. Sipuleucel-T immunotherapy for castration-resistant prostate cancer. *N Engl J Med* 2010;363:411–22.
8 Bol KF, Schreibelt G, Gerritsen WR, *et al*. Dendritic Cell-Based Immunotherapy: State of the Art and Beyond. *Clin Cancer Res* 2016;22:1897–906.
9 Lin MJ, Svensson-Arvelund J, Lubitz GS, *et al*. Cancer vaccines: the next immunotherapy frontier. *Nat Cancer* 2022;3:911–26.
10 Hammerich L, Bhardwaj N, Kohrt HE, *et al*. In situ vaccination for the treatment of cancer. *Immunotherapy (Los Angel)* 2016;8:315–30.
11 Inaba K, Turley S, Yamaide F, *et al*. Efficient Presentation of Phagocytosed Cellular Fragments on the Major Histocompatibility Complex Class II Products of Dendritic Cells. *J Exp Med* 1998;188:2163–73.
12 Catanzaro E, Feron O, Skirtach AG, *et al*. Immunogenic Cell Death and Role of Nanomaterials Serving as Therapeutic Vaccine for Personalized Cancer Immunotherapy. *Front Immunol* 2022;13:925290.
13 Doix B, Trempolec N, Riant O, *et al*. Low Photosensitizer Dose and Early Radiotherapy Enhance Antitumor Immune Response of Photodynamic Therapy-Based Dendritic Cell Vaccination. *Front Oncol* 2019;9:811.
14 Garg AD, Krysko DV, Vandenabeele P, *et al*. Hypericin-based photodynamic therapy induces surface exposure of damage-associated molecular patterns like HSP70 and calreticulin. *Cancer Immunol Immunother* 2012;61:215–21.
15 Mishchenko TA, Balalaeva IV, Turubanova VD, *et al*. Gold standard assessment of immunogenic cell death induced by photodynamic therapy: From in vitro to tumor mouse models and anti-cancer vaccination strategies. *Meth Cell Biol* 2024;183:203–64.
16 Trempolec N, Degavre C, Doix B, *et al*. Acidosis-Induced TGF-β2 Production Promotes Lipid Droplet Formation in Dendritic Cells and Alters Their Potential to Support Anti-Mesothelioma T Cell Response. *Cancers (Basel)* 2020;12:1284.
17 Trempolec N, Doix B, Degavre C, *et al*. Photodynamic Therapy-Based Dendritic Cell Vaccination Suited to Treat Peritoneal Mesothelioma. *Cancers (Basel)* 2020;12:545.
18 Pinto A, Mace Y, Drouet F, *et al*. A new ER-specific photosensitizer unravels (1)O2-driven protein oxidation and inhibition of deubiquitinases as a generic mechanism for cancer PDT. *Oncogene* 2016;35:3976–85.
19 Doix B, Bastien E, Rambaud A, *et al*. Preclinical Evaluation of White Led-Activated Non-porphyrinic Photosensitizer OR141 in 3D Tumor Spheroids and Mouse Skin Lesions. *Front Oncol* 2018;8:393.
20 Alzeibak R, Mishchenko TA, Shilyagina NY, *et al*. Targeting immunogenic cancer cell death by photodynamic therapy: past, present and future. *J Immunother Cancer* 2021;9:e001926.
21 Mishchenko TA, Balalaeva IV, Vedunova MV, *et al*. Ferroptosis and Photodynamic Therapy Synergism: Enhancing Anticancer Treatment. *Trends Cancer* 2021;7:484–7.
22 Rodrigues JA, Correia JH. Photodynamic Therapy for Colorectal Cancer: An Update and a Look to the Future. *Int J Mol Sci* 2023;24:12204.
23 Saji H, Song W, Furumoto K, *et al*. Systemic Antitumor Effect of Intratumoral Injection of Dendritic Cells in Combination with Local Photodynamic Therapy. *Clin Cancer Res* 2006;12:2568–74.
24 Jalili A, Makowski M, Świtaj T, *et al*. Effective Photoimmunotherapy of Murine Colon Carcinoma Induced by the Combination of Photodynamic Therapy and Dendritic Cells. *Clin Cancer Res* 2004;10:4498–508.
25 Wang W, Green M, Choi JE, *et al*. CD8+ T cells regulate tumour ferroptosis during cancer immunotherapy. *Nature New Biol* 2019;569:270–4.
26 Liao P, Wang W, Wang W, *et al*. CD8+ T cells and fatty acids orchestrate tumor ferroptosis and immunity via ACSL4. *Cancer Cell* 2022;40:365–78.
27 Wiernicki B, Maschalidi S, Pinney J, *et al*. Cancer cells dying from ferroptosis impede dendritic cell-mediated anti-tumor immunity. *Nat Commun* 2022;13:3676.
28 Efimova I, Catanzaro E, Van der Meeren L, *et al*. Vaccination with early ferroptotic cancer cells induces efficient antitumor immunity. *J Immunother Cancer* 2020;8:e001369.
29 Catanzaro E, Demuynck R, Naessens F, *et al*. Immunogenicity of ferroptosis in cancer: a matter of context? *Trends Cancer* 2024;10:407–16.
30 Demuynck R, Efimova I, Catanzaro E, *et al*. Ferroptosis: friend or foe in cancer immunotherapy? *Oncoimmunology* 2023;12:2182992.
31 Galluzzi L, Vitale I, Aaronson SA, *et al*. Molecular mechanisms of cell death: recommendations of the Nomenclature Committee on Cell Death 2018. *Cell Death Differ* 2018;25:486–541.
32 Dierge E, Debock E, Guilbaud C, *et al*. Peroxidation of n-3 and n-6 polyunsaturated fatty acids in the acidic tumor environment leads to ferroptosis-mediated anticancer effects. *Cell Metab* 2021;33:1701–15.
33 Sauter B, Albert ML, Francisco L, *et al*. Consequences of cell death: exposure to necrotic tumor cells, but not primary tissue cells or apoptotic cells, induces the maturation of immunostimulatory dendritic cells. *J Exp Med* 2000;191:423–34.
34 Albert ML, Pearce SFA, Francisco LM, *et al*. Immature Dendritic Cells Phagocytose Apoptotic Cells via αvβ5 and CD36, and Cross-present Antigens to Cytotoxic T Lymphocytes. *J Exp Med* 1998;188:1359–68.
35 Albert ML, Sauter B, Bhardwaj N. Dendritic cells acquire antigen from apoptotic cells and induce class I-restricted CTLs. *Nature New Biol* 1998;392:86–9.
36 Steinman RM, Turley S, Mellman I, *et al*. The induction of tolerance by dendritic cells that have captured apoptotic cells. *J Exp Med* 2000;191:411–6.
37 Shui S, Zhao Z, Wang H, *et al*. Non-enzymatic lipid peroxidation initiated by photodynamic therapy drives a distinct ferroptosis-like cell death pathway. *Redox Biol* 2021;45:102056.
38 Dudek AM, Martin S, Garg AD, *et al*. Immature, Semi-Mature, and Fully Mature Dendritic Cells: Toward a DC-Cancer Cells Interface That Augments Anticancer Immunity. *Front Immunol* 2013;4:438.
39 Janssen EM, Droin NM, Lemmens EE, *et al*. CD4+ T-cell help controls CD8+ T-cell memory via TRAIL-mediated activation-induced cell death. *Nature New Biol* 2005;434:88–93.

40 Cox MC, Castiello L, Mattei M, *et al*. Clinical and Antitumor Immune Responses in Relapsed/Refractory Follicular Lymphoma Patients after Intranodal Injections of IFNα-Dendritic Cells and Rituximab: a Phase I Clinical Trial. *Clin Cancer Res* 2019;25:5231–41.
41 Rozera C, Cappellini GA, D'Agostino G, *et al*. Intratumoral injection of IFN-alpha dendritic cells after dacarbazine activates anti-tumor immunity: results from a phase I trial in advanced melanoma. *J Transl Med* 2015;13:139.
42 Kolstad A, Kumari S, Walczak M, *et al*. Sequential intranodal immunotherapy induces antitumor immunity and correlated regression of disseminated follicular lymphoma. *Blood* 2015;125:82–9.
43 Lee JM, Lee M-H, Garon E, *et al*. Phase I Trial of Intratumoral Injection of *CCL21* Gene-Modified Dendritic Cells in Lung Cancer Elicits Tumor-Specific Immune Responses and $CD8^+$ T-cell Infiltration. *Clin Cancer Res* 2017;23:4556–68.
44 Dhodapkar MV, Sznol M, Zhao B, *et al*. Induction of antigen-specific immunity with a vaccine targeting NY-ESO-1 to the dendritic cell receptor DEC-205. *Sci Transl Med* 2014;6:232ra51.
45 Bonifaz LC, Bonnyay DP, Charalambous A, *et al*. In vivo targeting of antigens to maturing dendritic cells via the DEC-205 receptor improves T cell vaccination. *J Exp Med* 2004;199:815–24.
46 Henrickson SE, Perro M, Loughhead SM, *et al*. T cell-dendritic cell interaction kinetics and memory fate decisions. *Immunity* 2013;39:496–507.
47 Kraemer AI, Chong C, Huber F, *et al*. The immunopeptidome landscape associated with T cell infiltration, inflammation and immune editing in lung cancer. *Nat Cancer* 2023;4:608–28.
48 Laureano RS, Sprooten J, Vanmeerbeerk I, *et al*. Trial watch: Dendritic cell (DC)-based immunotherapy for cancer. *Oncoimmunology* 2022;11:2096363.
49 Roney K. Bone marrow-derived dendritic cells. *Methods Mol Biol* 2013;1031:71–6.
50 Hiasa M, Abe M, Nakano A, *et al*. GM-CSF and IL-4 induce dendritic cell differentiation and disrupt osteoclastogenesis through M-CSF receptor shedding by up-regulation of TNF-alpha converting enzyme (TACE). *Blood* 2009;114:4517–26.
51 Susaki EA, Tainaka K, Perrin D, *et al*. Advanced CUBIC protocols for whole-brain and whole-body clearing and imaging. *Nat Protoc* 2015;10:1709–27.
52 Huyghe N, Benidovskaya E, Beyaert S, *et al*. Multiplex Immunofluorescence Combined with Spatial Image Analysis for the Clinical and Biological Assessment of the Tumor Microenvironment. *J Vis Exp* 2023;2023:196.
53 Zhu J, Naulaerts S, Boudhan L, *et al*. Tumour immune rejection triggered by activation of α2-adrenergic receptors. *Nature New Biol* 2023;618:607–15.

SUPPLEMENTARY MOVIES

Suppl. movie 1. Representative 3D light sheet microscopy videos depicting propidium iodide-positive dead cells (red) and counterstained nuclei (blue) within CT26 spheroid **(A)** in the absence of PDT, **(B)** 6h after PDT (100 nM PS OR141) and **(C)** after PDT but in the presence of Ferrostatin-1. Respective incubation times are described in Figure 1 legend. Scale bar: 70µm

Suppl. movie 2. (A) Representative staining and modeling derived from light sheet microscopy-based reconstructions on Imaris program, depicting infiltration of $CD11c^+$ iDC (red) in CT26 spheroids 6h after PDT (100 nM PS OR141). Nuclei are counterstained with Hoechst (A, blue) and delimit the spheroid volume. **(B-D)** Image reconstructions depicting infiltration of $CD11c^+$ iDC (red) in **(B)** untreated CT26 spheroids, **(C)** 6h after PDT (100 nM PS OR141) and **(D)** after PDT but in the presence of Ferrostatin-1. Respective incubation times are described in Figure 2 legend. Scale bar: 100µm.

Suppl. Figure 1

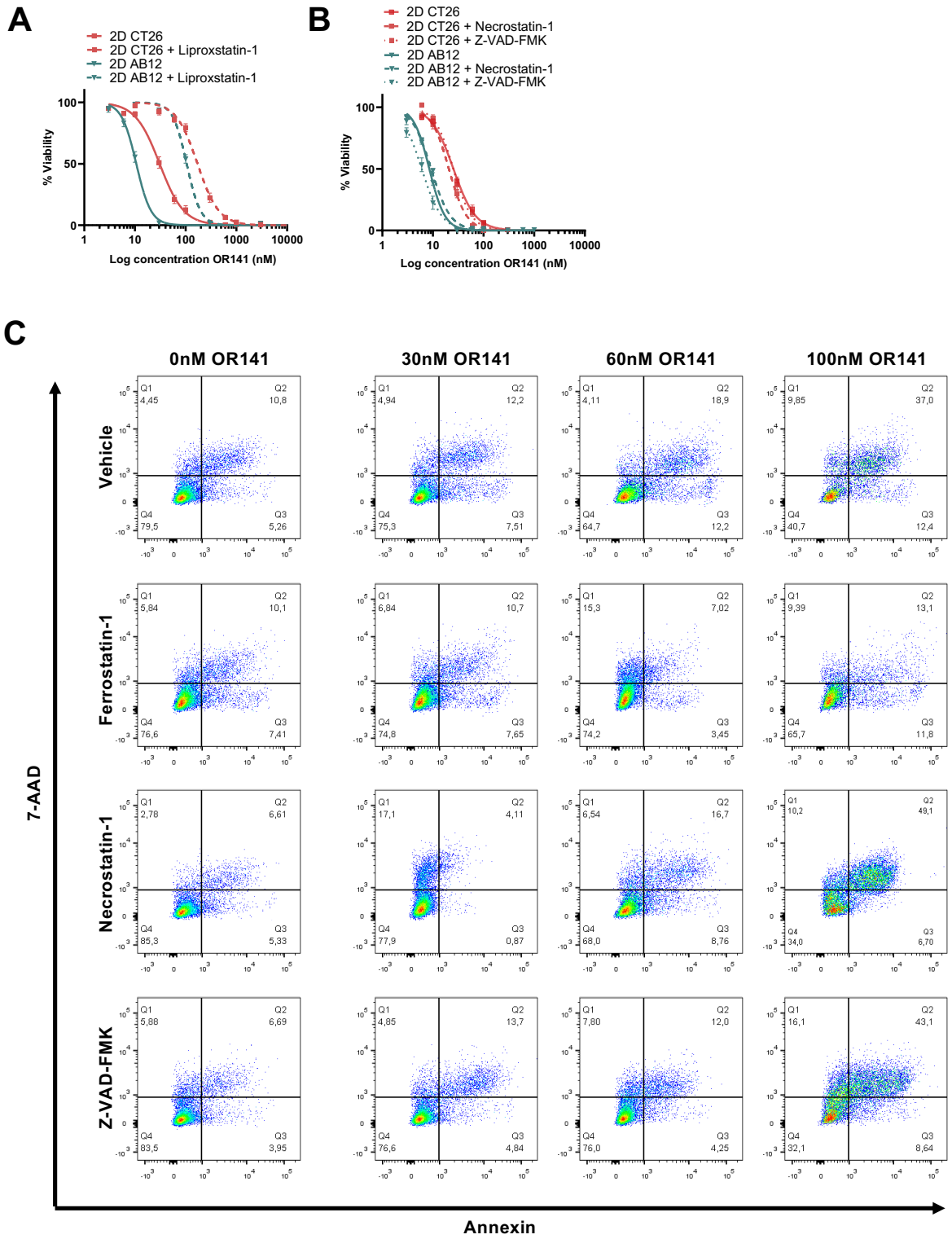

Suppl. Figure 1. PDT induces ferroptosis in cancer cells. CT26 colorectal carcinoma and AB12 mesothelioma 2D cell cultures and 3D spheroids were treated with the following drugs: ferrostatin-1 (10µM), liproxstatin-1 (10µM), necrostatin-1 (20 µM for 2D and 30µM for 3D), Zvad-fmk (25 µM for 2D or 40µM for 3D). After 48h pre-treatment, cell cultures or spheroids were incubated with PS-OR141 in the dark for 1 hour (2D) or 4 hours (3D) at the indicated concentrations, followed by a washing step. Photoactivation was performed using a LED light source for 60 min (2D) or 90 min (3D) and incubation was continued after the renewal of cell death inhibitors. **(A-B)** Dose-response curves depicting the viability of CT26 and AB12 2D cells (PrestoBlue) 24h post-PDT in the presence of (A) 10 µM liproxstatin-1 or (B) 20µM necrostatin-1 or 25µM ZVAD-FMK. **(C)** Representative annexin V/ 7-AAD flow cytometry analysis 1h post-PDT from dissociated CT26 spheroids. Data are plotted as the means ± SEM from 3 independent experiments performed with ≥3 technical replicates; when spheroids are involved, min. 6 spheroids were pooled together per condition.

Suppl. Figure 2

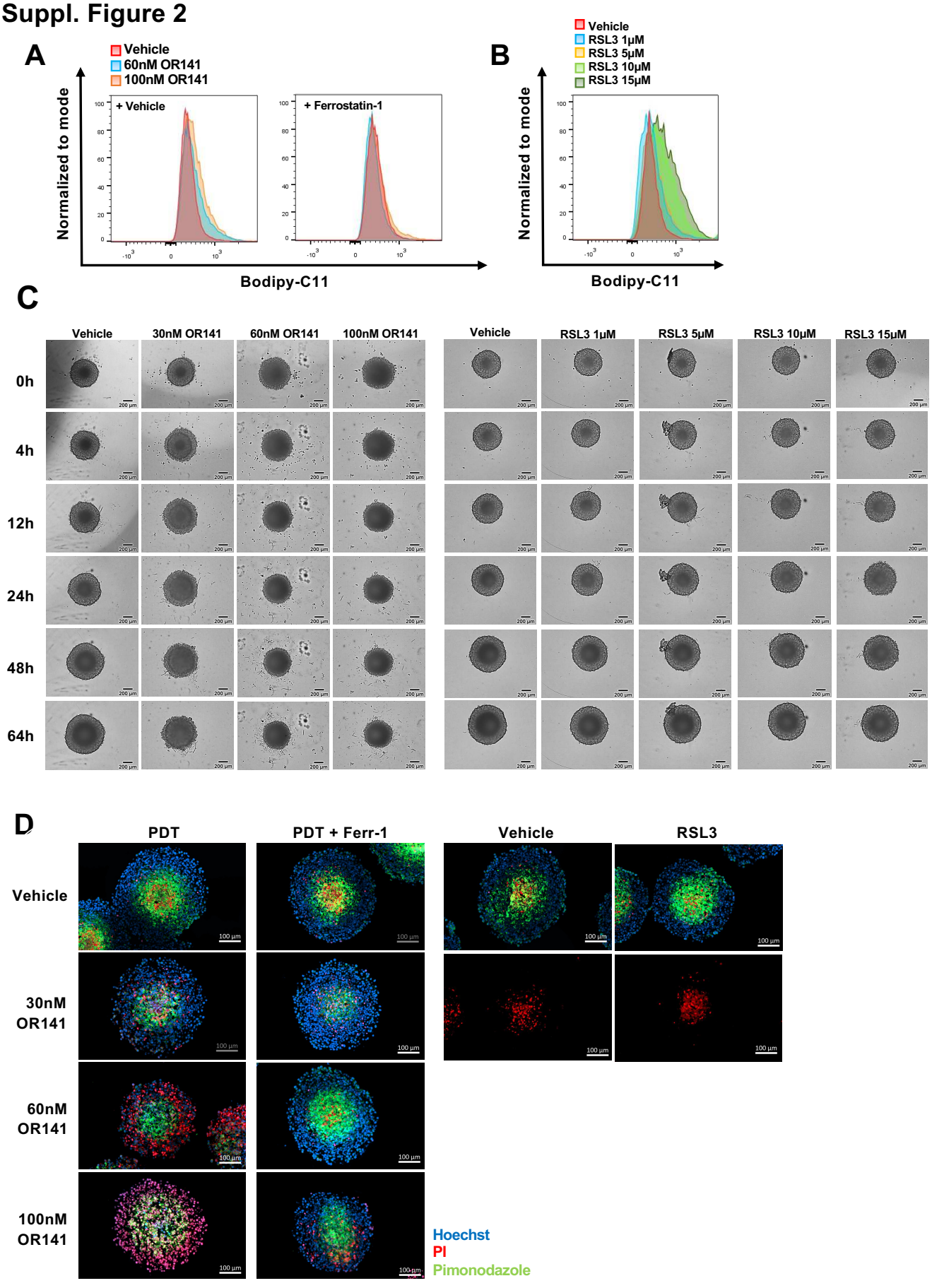

Suppl. Figure 2. PDT induces lipid peroxidation and inhibits spheroid outgrowth. CT26 3D spheroids were pre-treated with 10 µM ferrostatin-1 and incubated 48h later with PS OR141 in the dark for 4 hours, followed by a washing step. Photoactivation was performed using a LED light source for 90 minutes and incubation was continued after the renewal of ferrostatin-1 for 20h. A similar protocol was applied for RSL3 treatment with 48h pre-treatment and renewal for final 48h-incubation. **(A-B)** Flow cytometry-based lipid peroxidation measurements from CT26 spheroids (A) post-PDT in the absence (left panel) or presence (right panel) of 10 µM ferrostatin-1 and (B) post-RSL3 treatment. **(C)** Representative phase-contrast images (Incucyte) showing the effects of PDT or RSL3 treatment on CT26 spheroids over time. Scale bar: 200 µm. **(D)** Representative immunofluorescence staining for hypoxia marker pimonidazole (green), dead cells stained with propidium iodide (red) and Hoechst-counterstained nuclei (blue) in CT26 3D spheroids treated as indicated. Scale bar: 100µm. Data are representative of 3 independent experiments performed with ≥6 technical replicates.

Suppl. Figure 3

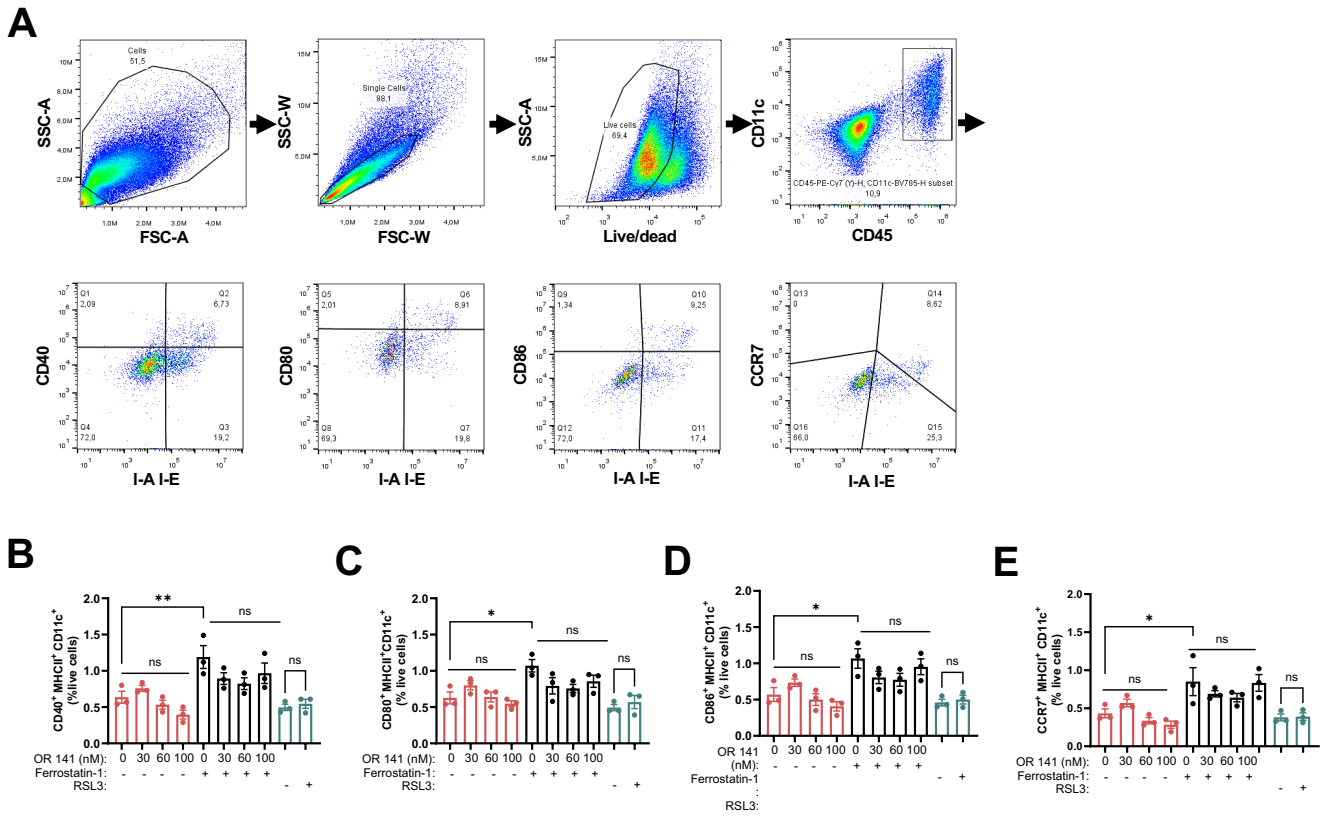

Suppl. Figure 3. PDT promotes iDC infiltration in 3D spheroids. Maturation analysis of DCs isolated from CT26 spheroids after exposure to either photoactivated PS OR141 in the presence (or not) of 10 µM ferrostatin-1 or to the ferroptosis inducer RSL3 (5µM). **(A)** Gating strategy for the maturation analysis of CD11c⁺ cells. Doublets and dead cells were excluded before analyzing MHCII⁺ CD11⁺ CD45⁺ populations for CD40⁺, CD80⁺, CD86⁺, and CCR7⁺ expression (FlowJo software). **(B-E)** Flow cytometry-based quantification of infiltrated MHCII⁺ CD11⁺ CD45⁺ cells and associated changes in the expression of co-stimulatory molecules CD40 (B), CD80 (C), CD86 (D), and CCR7 (E) 48 hours after iDC transfer. Data are presented as means ± SEM (*p ≤ 0.05; **p ≤ 0.01; ***p ≤ 0.001; ****p ≤ 0.0001; ns, not significant) from 3 independent experiments, each with ≥3 technical replicates. For spheroid experiments, a minimum of 6 spheroids were pooled per condition. Significance was determined using one-way ANOVA with Tukey's multiple comparison test.

Suppl. Figure 4

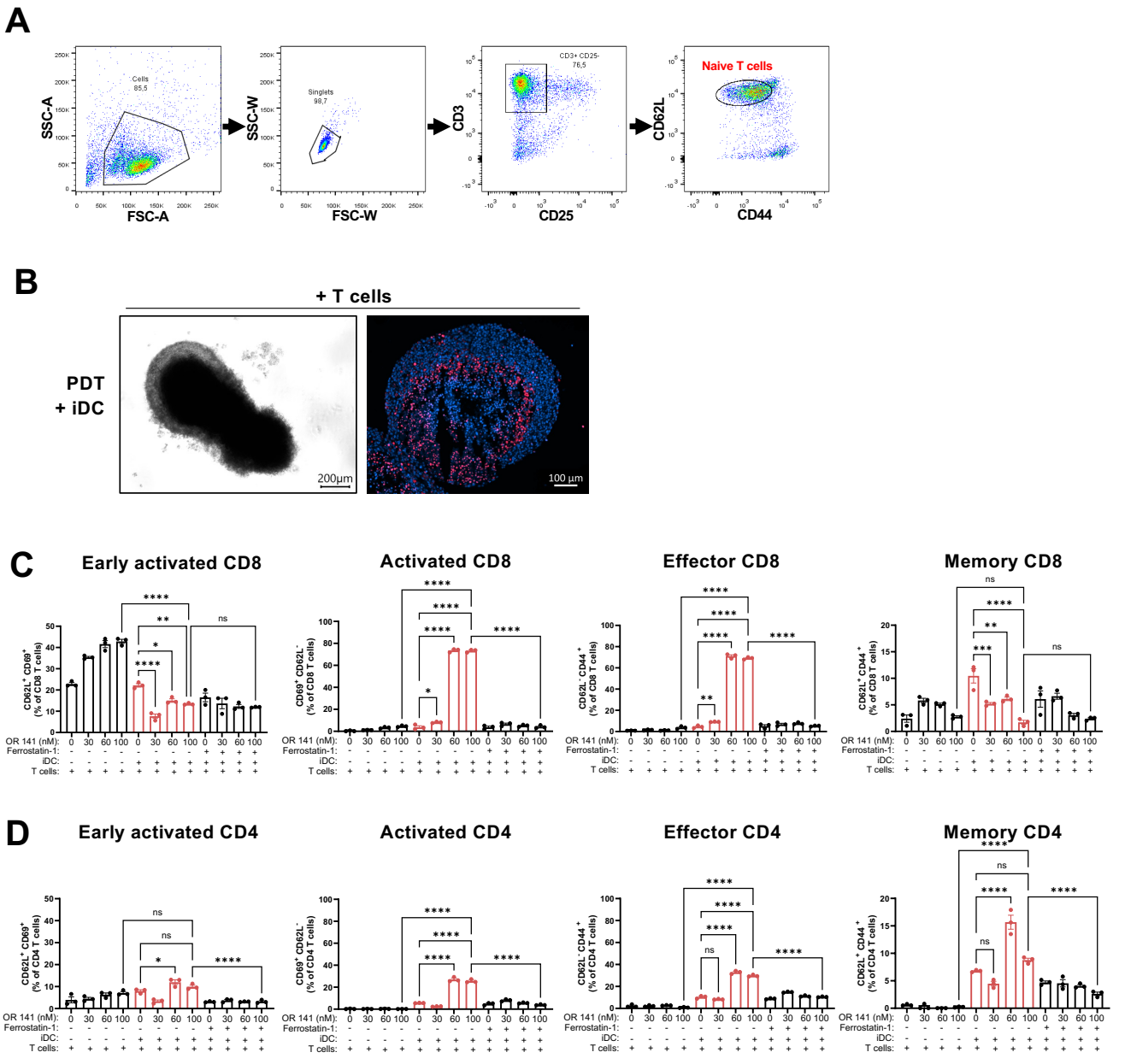

Suppl. Figure 4

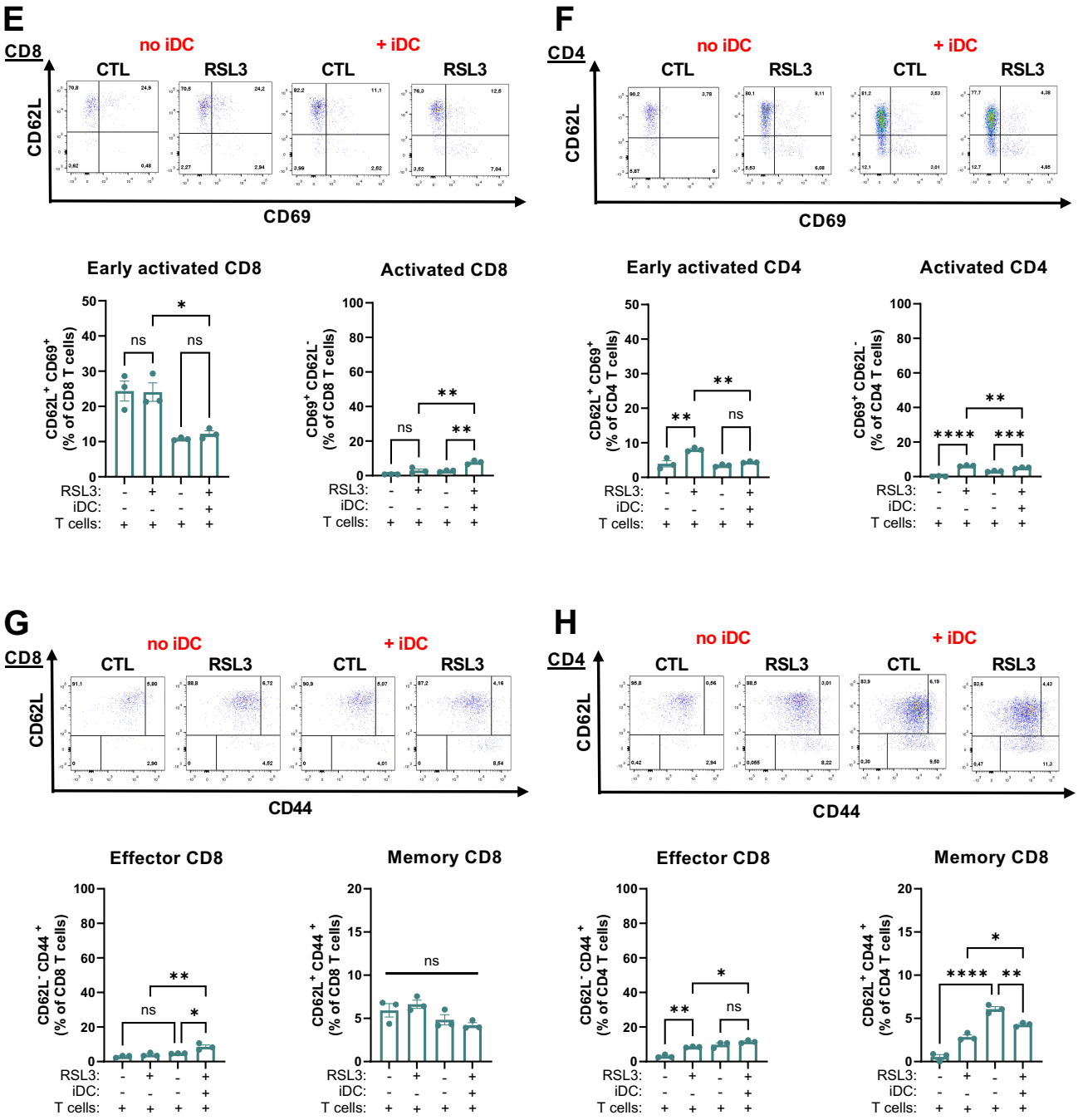

Suppl. Figure 4. PDT, but not ferroptosis inducer RSL3, promotes DC-mediated T cell response against 3D spheroids. Immune response evaluation 6 days after naive T cell adoptive transfer consecutively to the iDC transfer to PDT or RSL3-exposed spheroids. CT26 3D spheroids were pre-treated with 10 µM ferrostatin-1 and incubated 48h later with PS OR141 in the dark for 4 hours, followed by a washing step. Photoactivation was performed using a LED light source for 90 minutes and incubation was continued after the renewal of ferrostatin-1. A similar protocol was applied for RSL3 treatment with 48h pre-treatment and renewal for final incubation. Exogenous iDC ($5x10^3$ per spheroid) were added 48h post-PDT or after the last RSL3 addition, followed 48h later by addition of $CD62L^+$ $CD44^-$ $CD25^-$ $CD3^+$ lymphocytes (5.10^3 per spheroid); cytotoxic activity was analyzed 6 days later. **(A)** Gating strategy for naive T cell ($CD62L^+$ $CD25^-$ $CD44^-$ $CD3^+$) sorting on BD FACSAria III Cell Sorter (BD Biosciences). Cells were first sorted based on size and granularity and doublet cells were excluded. **(B)** Representative phase-contrast pictures (left panel, scale bar: 200µm) and fluorescence pictures depicting propidium iodide positive (red) signal (right panel, scale bar: 100µm) from CT26 spheroids treated as indicated and revealing the loss of spheroid integrity and associated extrusion of central dead cells. **(C-H)** Quantification of flow cytometry-based phenotyping of $CD8^+$ and $CD4^+$ T cells using CD44, CD62L and CD69 markers from 3D spheroids (C-D) post-PDT treatment or (E-H) after RSL3 exposure. Data are representative of 3 independent experiments (with ≥ 6 technical replicates). Data are plotted as the means ± SEM (*, $p \leq 0.05$; **, $p \leq 0.01$; ***, $p \leq 0.001$; ****, $p \leq 0.0001$; ns, $p > 0.05$) from 3 independent experiments performed with ≥3 technical replicates (min. 6 spheroids were pooled together per condition). Significance was determined by one-way ANOVA with Tukey's multiple comparison test.

Suppl. Figure 5

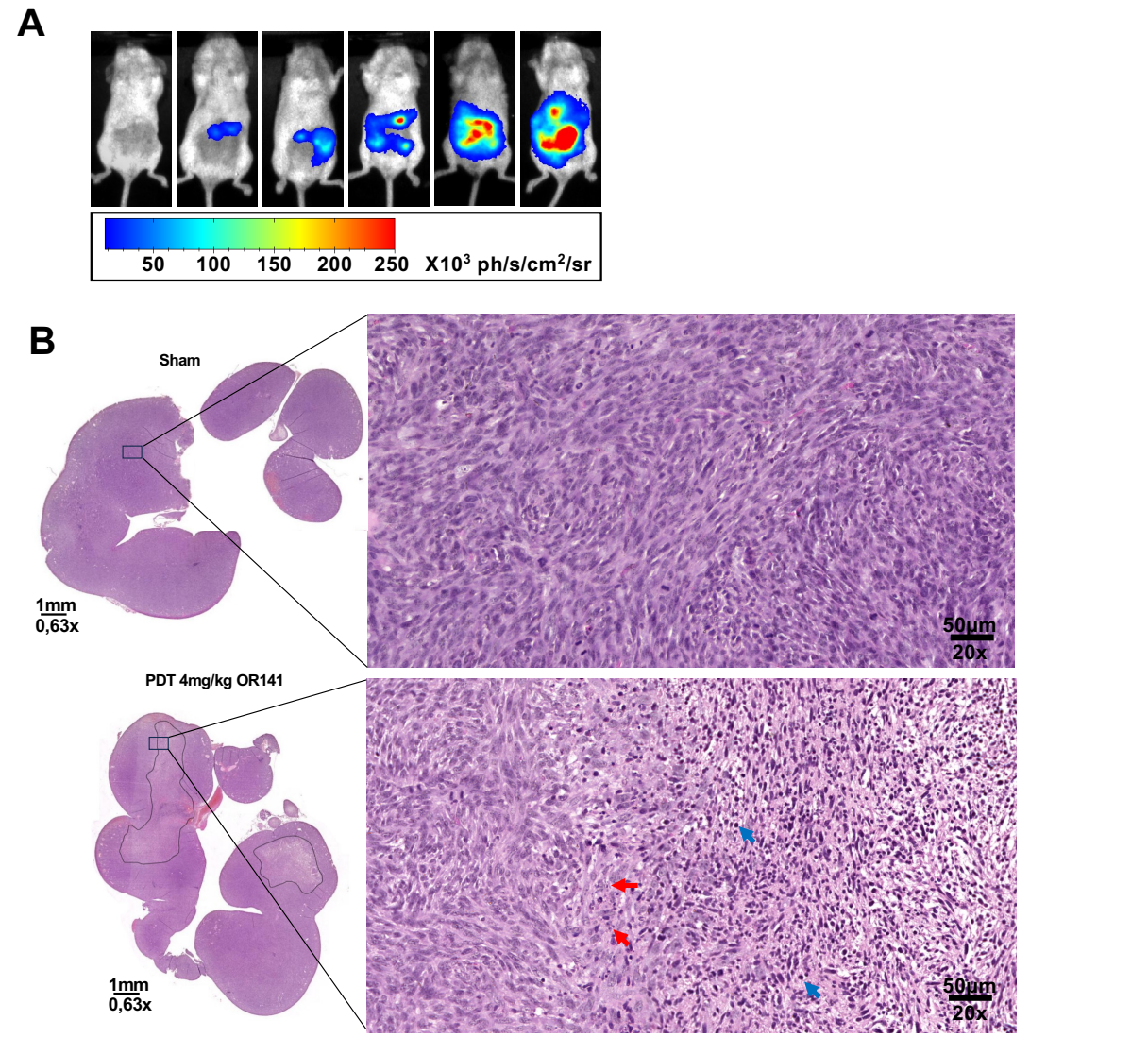

Suppl. Figure 5

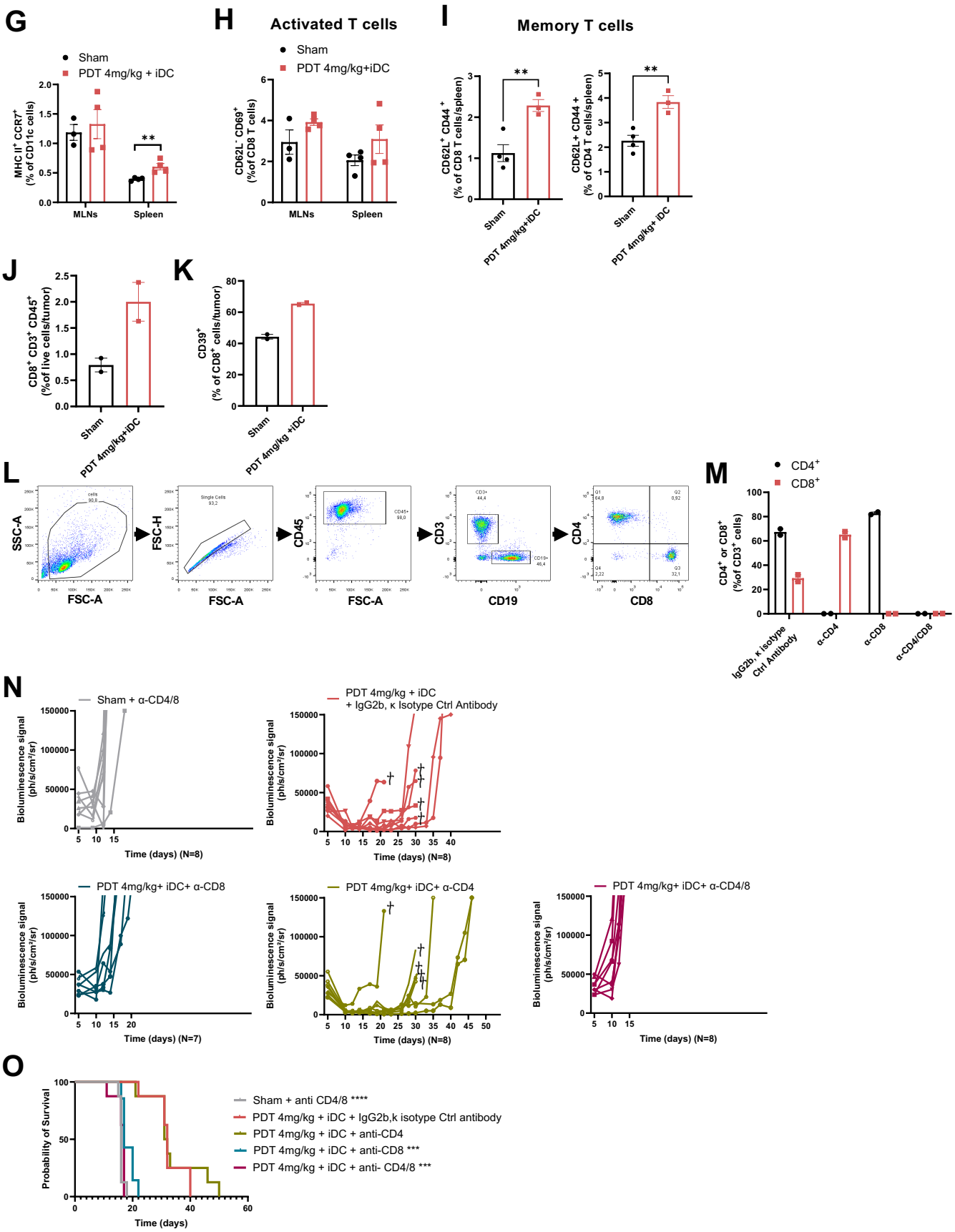

Suppl. Figure 5. Laparoscopic PDT administration promotes iDC-based memory immune response against peritoneal tumors. Balb/CByJ mice were i.p. injected with 1x10^6 luciferase-positive AB1 tumor cells and exposed 7 days later to PDT. PS-OR141 (0.4 or 4 mg/kg) was injected i.p. 90 min before laparoscopy and photo-activated for 15 min upon endoscopal light exposure; sham animals were used as controls. Where indicated, iDC (2×10^6) were injected i.p. 60 min after in situ PDT. **(A)** Bioluminescence-based imaging depicting time course progression of peritoneal carcinomatosis, expressed in photons/second/cm²/steradian (ph/s/cm²/sr). **(B)** Histological analysis of FFPE tumor sections stained with hematoxylin and eosin from PDT-treated mice (6 days post-treatment) (scale bar: 1mm); magnified panel from a representative tumor section highlights an hypereosinophilic region showing cell death (red arrows) and immune cell infiltration (blue arrows) (scale bar: 50µm). **(C)** Weight monitoring of mice bearing luc$^+$ AB1 tumors and i.p. injected with 2x10^6 iDCs or exposed to in situ intraperitoneal PDT (4mg/kg PS OR141), or a combination of both. N = 6 mice per group. **(D)** Kaplan-Meier survival curves of mice treated as indicated. N = 6-8 mice per group. Significance was determined with log-rank (Mantel-Cox) test (*, p≤0.05). **(E)** Tumor burden monitored by bioluminescence (expressed as photons/s/cm^2/sr) and **(F)** corresponding survival curves of mice exposed in situ to PDT and iDC at late timing (day 15 post-tumor injection vs. day 7 in Figure 5). In **(F)**, arrow at day 52 indicates rechallenge by i.p. injection of 1×10^6 luciferase-positive AB1 tumor cells. N= 4-6 mice per group. Significance was determined with log-rank (Mantel-Cox) test (*, p≤0.05). **(G-I)** Immune cell activation analysis carried out by flow cytometry from mesenteric lymph nodes and spleens collected 10 days after treatment. Bar graphs represent (G) CCR7$^+$ MHCII$^+$ CD11$^+$ cells, **(H)** activated CD62L$^-$ CD69$^+$ CD8$^+$ T cells, and **(I)** (spleen) memory CD62L$^+$ CD44$^+$ CD8$^+$ and CD4$^+$ T cells in PDT 4mg/kg + iDC experimental condition (vs. sham mice). Data are plotted as the means ± SEM (**, p≤0.01; ns, p > 0.05) from 3 to 4 mice per group. Significance was determined by Student's t test. **(J)** Flow cytometry-based quantification of infiltrated CD8$^+$ T cells and **(K)** CD39$^+$ CD8$^+$ T cells in tumors collected at ethical end point in PDT 4mg/kg + iDC experimental condition (vs. sham mice). N=2 mice per group. **(L-M)** Evaluation of T cell involvement in the immune response to PDT+iDC treatment. (L) Gating strategy for flow cytometry to assess CD4$^+$ and CD8$^+$ T cell depletion. Cells were first sorted based on size and granularity and doublet cells were excluded. (M) Flow cytometry data confirming efficient T cell depletion 30 hours post-first injection of depleting antibodies (vs. control IgG2 antibodies). **(N)** Tumor burden monitored by bioluminescence (expressed as photons/s/cm2/sr) and **(O)** corresponding survival curves of mice treated as indicated and depleted (or not) in CD4$^+$ and/or CD8$^+$ T cells 24h before treatment initiation. Experimental endpoint was determined when mice reached the ethical limits or euthanasia (†) upon major ascite accumulation. N=8 mice per group. Significance was determined with log-rank (Mantel-Cox) test (****, p ≤ 0.0001 vs. control IgG2 condition).

Suppl. Figure 6

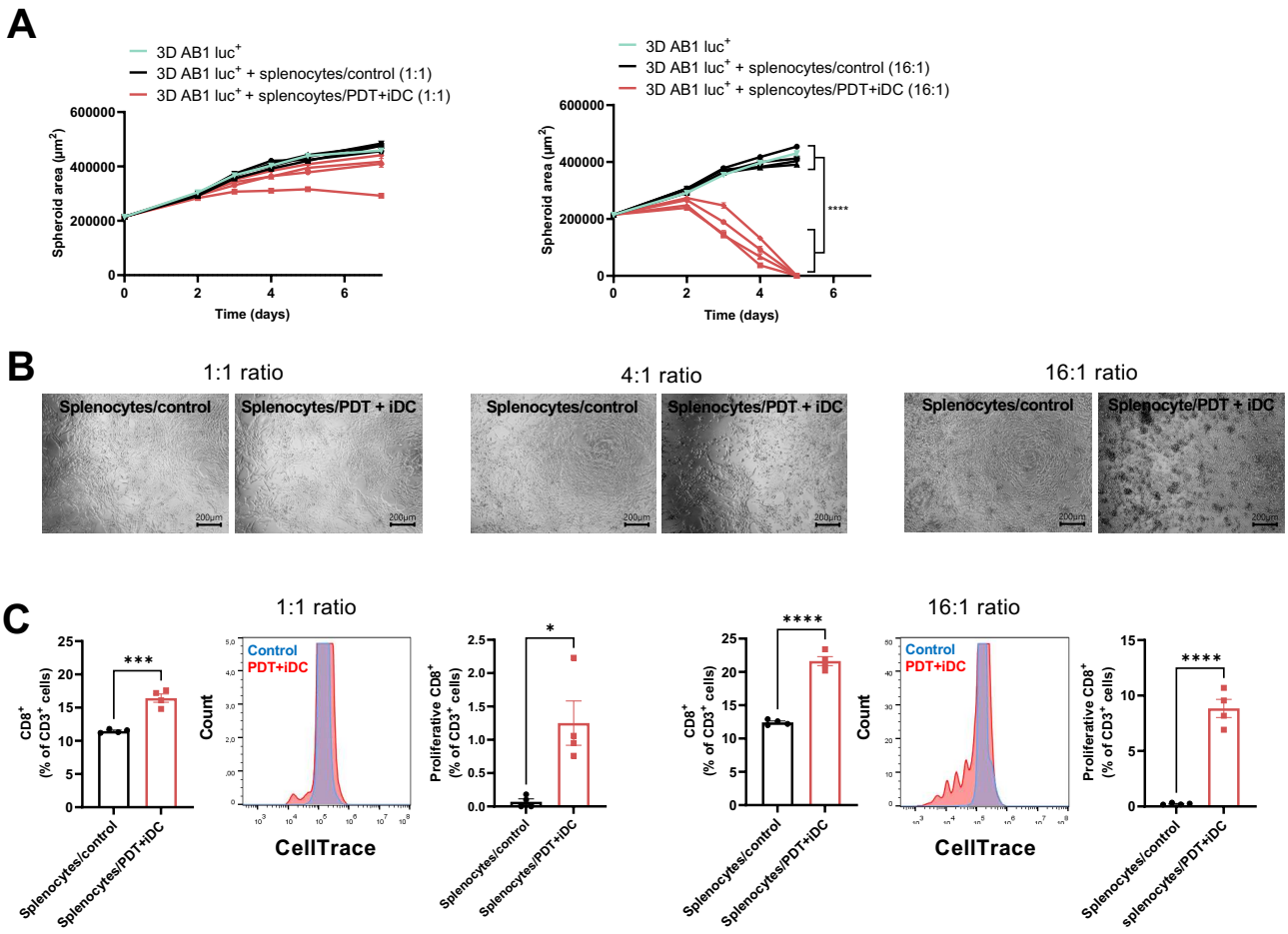

Suppl. Figure 6. PDT combined with adoptive transfer of iDC induces ex vivo immune memory response. (A) Splenocytes were collected from vaccinated (surviving at day 130) or naive mice and exposed to AB1 cell monolayers ($3x10^3$ cells plated 24h before) or spheroids ($5x10^3$ cells plated 3 days before) at different effector to target ratios (i.e., 1:1, 4:1 or 16:1, determined based on cancer cell numbers at the time of plating). **(A-B)** Immune response was evaluated using luc+ AB1 spheroids co-cultured for 7 days with splenocytes, at effector to target ratios of (A) 1:1 and (B) 16:1. **(C)** Representative phase-contrast pictures depicting development of cytotoxicity in 2D luc+ AB1 cancer cell culture at the indicated effector to target ratios. **(D)** Percentage and proliferation (Celltrace violet-stained, flow cytometry) of CD8 T cells after 3 days of exposition to 2D luc+ AB1 cells at the indicated effector to target ratios. Data are plotted as the means ± SEM (*, $p \leq 0.05$; ***, $p \leq 0.001$; ****, $p \leq 0.0001$; ns, $p > 0.05$) from 3 independent experiments performed with ≥3 technical replicates; when spheroids are involved, min. 6 spheroids were pooled together per condition. Significance was determined by Student's t test.